The role of Fgf10/Fgfr2b signaling during lung development

Inaugural Dissertation
Submitted to the
Faculty of Medicine
In partial fulfillment of the requirements
for the **Dr. med**. – Degree
Of the Faculty of Medicine of the
Justus Liebig University Giessen
Germany

by
Jamschid Sedighi
of
Depajak, Afghanistan

Gießen 2021

Of the Faculty of Medicine of the Justus Liebig University Giessen
from the Department of Internal Medicine II and
Excellence Cluster Cardio-Pulmonary System (ECCPS)

First Supervisor: **PD Dr. Chao**
Second Supervisor: **Prof. Dr. Pullamsetti**

Date of Doctoral Defense: 13th of June 2022

Dedicated to my parents Alem und Masuda Sedighi

من این رساله را به پدر و مادر عزیزم تقدیم میکنم

پدر جان و مادر جان عزیزم برای تشکری به دنبال قشنگ ترین واژه ها و کلمات میگردم

اما واژه ها آنقدر فقیر و کم بضاعت هستند

فقط میگویم دوست تان دارم و در این دو کلمه دنیای نهفته است.

امید دارم بتوانم قدردان زحمات تان باشم

به خاطرتمام خوبی های که در حق من کردید

و به من بال و پر دادید و من را بالنده کردید

و با سوختن خود عشق و شور را در وجودم روشن کردید

یک کهکشان از زحمات تان در قبال بنده تشکری میکنم

همیشه درخت عمر تان سرسبز و پر ثمر باشد

از خداوند متعال خواهانم جنت فردوس را نصیب تان گرداند.

Declaration

“I declare that I have completed this dissertation single-handedly without the unauthorized help of a second party and only with the assistance acknowledged therein. I have appropriately acknowledged and referenced all text passages that are derived literally from or are based on the content of published or unpublished work of others, and all information that relates to verbal communications. I have abided by the principles of good scientific conduct laid down in the charter of the Justus Liebig University of Giessen in carrying out the investigations described in the dissertation.”

_____ _____

Place, Date Jamschid Sedighi

List of Contents

List of Figures:

List of Tables:

Abbreviations and acronyms

α-SMA	α -Smooth Muscle Actin
ADRP	Adipose differentiation-related protein
AEC I	Alveolar epithelial cell type I
AEC II	Alveolar epithelial cell type II
ALSG	Aplasia of lacrimal and salivary glands
BADJ	Broncho-alveolar duct junction
BMP 4	Bone morphogenetic protein 4
BPD	Bronchopulmonary dysplasia
BSA	Bovine serum albumin
CCSP	Club cell secretary protein
COPD	Chronic obstructive pulmonary disease
E	Embryonic
FGF10	Fibroblast growth factor
FGFR	Fibroblast growth factor receptor
GFP	Green fluorescent protein
HBSS	Hanks balanced salt solution
HOX	Hyperoxia
HRP	Horseradish peroxidase

ID2	Inhibitor of differentiation 2
LADD	Lacrimo-auriculo-dento-digital syndrome
LIF	Lipofibroblast
MYF	Myofibroblast
NF-κB	Nuclear factor 'kappa-light-chain-enhancer' of activated B-cells
NOX	Normoxia
P	Postnatal
PBS	Phosphate-buffered saline
PDGF	Platelet derived growth factor
PDPN	Podoplanin
PECAM	Platelet endothelial cell adhesion molecule
PFA	Paraformaldehyde
RA	Retinoid acid
SCGB1A1	Secretoglobin, Family1A, Member 1
SDS	Sodium dodecyl sulfate
SEM	Subepithelial mesenchyme
SFTPC	Surfactant protein C
SFTPB	Surfactant protein B
SHH	Sonic hedgehog Abbreviations and Acronyms vi

SMM	Submesothelial mesenchyme
SOX 9 SRY	(sex determining region Y)-box 9
SP1	Specificity Protein 1
SPRY 2	Sprouty 2
TAE	TRIS-Acetate-EDTA
TBS-T	TRIS-buffered saline with Tween 20
TGF-β1	Transforming growth factor □-1
VEGF	Vascular endothelial growth factor
VEGFR	Vascular endothelial growth factor receptor
WNT	Wingless and int

1. INTRODUCTION

Primary research on embryonic lung development provides a rare opportunity to make important discoveries that will impact the future health of humans. In order to find a deeper understanding of cellular and molecular processes in lung development, mouse lungs were used due to the proximity of their genome and physiology to humans, making them a suitable substitute.

1.1. Lung development: human compared to mouse

Lung development in humans begins after four weeks of gestation. From the laryngo-tracheal groove, the ventral wall of the caudal primitive foregut starts to develop and forms a pouch like structure. The prospective trachea detaches, during the subsequent growth of the lung, from the foregut by the creation of the so-called tracheo-esophageal septum. Afterward, the most distal part of the tracheal tube divides into two buds, forms the right and left primary bronchial buds. These primary buds are further branching to form three secondary bronchial buds on the right and then two secondary bronchial buds respectively on the left side. These buds are the starting point of the five lobes in the mature lung (Moore et al. 2016).

The human lung consists of two lobes on the left and three lobes on the right side. In contrast, the mouse lung has only one lobe on the left and four lobes on the right side.

Lung development in mice begins at embryonic day 8 (E8). It involves several signaling molecules like Fibrotic growth factor 1 (Fgf1) and Fgf2 from the cardiac mesoderm, which express the transcription factor Nkx2.1 (Ttf1). The Nkx2.1-positive cells originating from the mesoderm are the origin cells of the lung. Finally, out of this population Sox2 expressing cells belonging to the anterior foregut and cells from the dorsal foregut emerge, whereas the anterior foregut related cells form the future trachea and the paired main bronchi (Weinstein et al. 1998).

The whole mouse and human lung development contains of four stages (Chao et al. 2015, Figure 1). These four histologically and morphologically distinguishable stages are divided in pseudoglandular, canalicular, saccular and alveolar stages.

The murine pseudoglandular stage starts at embryonic day 9.5 (E9.5) and continues until embryonic day 16.5 (E16.5) whereas the human pseudoglandular stage occurs from

gestation week 4 until 17. As the name suggests, the formation of the branches resulting from the branching morphogenesis resembles exocrine glands. At this point several mesenchymal and epithelial progenitor cells evolve.

The characterization of this stage is the branching morphogenesis where the basic tree-like structure of the airways is made by subdivision of the airways.

Following the canalicular stage from E16.5 to E17.5 in mice and gestation week 17-26 in humans, it comes to further expansion in the respiratory tree, accompanied by vascularization and angiogenesis along the airway. At this stage, the alveolar bipotent progenitor cells differentiate to alveolar epithelial cells type I (AEC I) and type II (AEC II) (Treutlein et al. 2014). In the developed lung, the AEC I cell with their elongated, squamous shape form the surface of the alveoli and build the gas exchange units of the lung (Makanya et al. 2013). The AEC II cells produce and secrete surfactant to reduce the tension of the alveolar surface, preventing the alveoli from collapsing (El Agha and Bellusci 2014). Although the AEC I cells cover 96% of the lung they are less numerous than the rather cuboidal AEC II (Desai et al. 2014; Hou et al. 2015).

The saccular stage takes place from E17.5 to postnatal day 5 (P5) in mice and from gestational week 26-36 in humans. The formation of the alveolar sac occurs by the thinning of the mesenchymal layer (formation of primary septa) as a result of apoptosis. The distance between the capillary and alveolar lumen decreases, enabling better conditions for gas exchange in terms of reduced distance for gas diffusion (Kresch et al. 1998) and of the ongoing branching process. From this point onwards the lung provides conditions for gas exchange: the alveolar sacs as the alveolar prestige marks the gas exchanging unit with the associated capillaries. Surfactant as a byproduct of AEC II and lipofibroblast (LIF) stabilizes the alveoli by reducing the tension on the surfactant (Wang et al. 2016).

The alveolar stage, which is the final step in lung development, starts from P5 to P30 in mice and begins already before birth from gestational week 36 in humans. The so-called secondary septa formation is responsible for the alveolarization process. Secondary septa subdivide the alveola into many mature alveoli and therefore increase the gas exchange surface to around 82 cm^2 (about 2.3 Mio. alveoli) for mice (Knust et al. 2009).

From the wall of the alveolar sac, the secondary septa formation begins with the deposition of elastin in primary septa (wall of alveolar sacs). Afterwards, secondary septa

arise at the place of elastin deposition and extends towards the alveolar sac airspace to subdivide it into the smallest respiratory units of the lung mature alveoli (Chao et al. 2016).

The process of alveolarization takes the first six months after birth in humans (Schittny et al. 2008). The alveolar myofibroblasts, which are localized in the mesenchyme at the tip of the emerging secondary septa, are responsible for the secondary septa formation (El Agha and Bellusci 2014).

The developmental processes of the lung are divided into the branching morphogenesis program from E9.5 until E16.5 and followed by the alveolar epithelial differentiation program (Chang et al. 2013).

As we have seen, the alveolar stage in mice begins after birth and in humans starts in the embryonic stage already. This difference is an important factor for showing that the BPD mouse model greatly applies to the study of pathological processes in the context of BPD: a scheduled birth in mice corresponds to a preterm birth in humans. So, when applying oxygen to mice after birth, this is equivalent to oxygen application in preterm humans, as at this stage humans normally still remain in the womb.

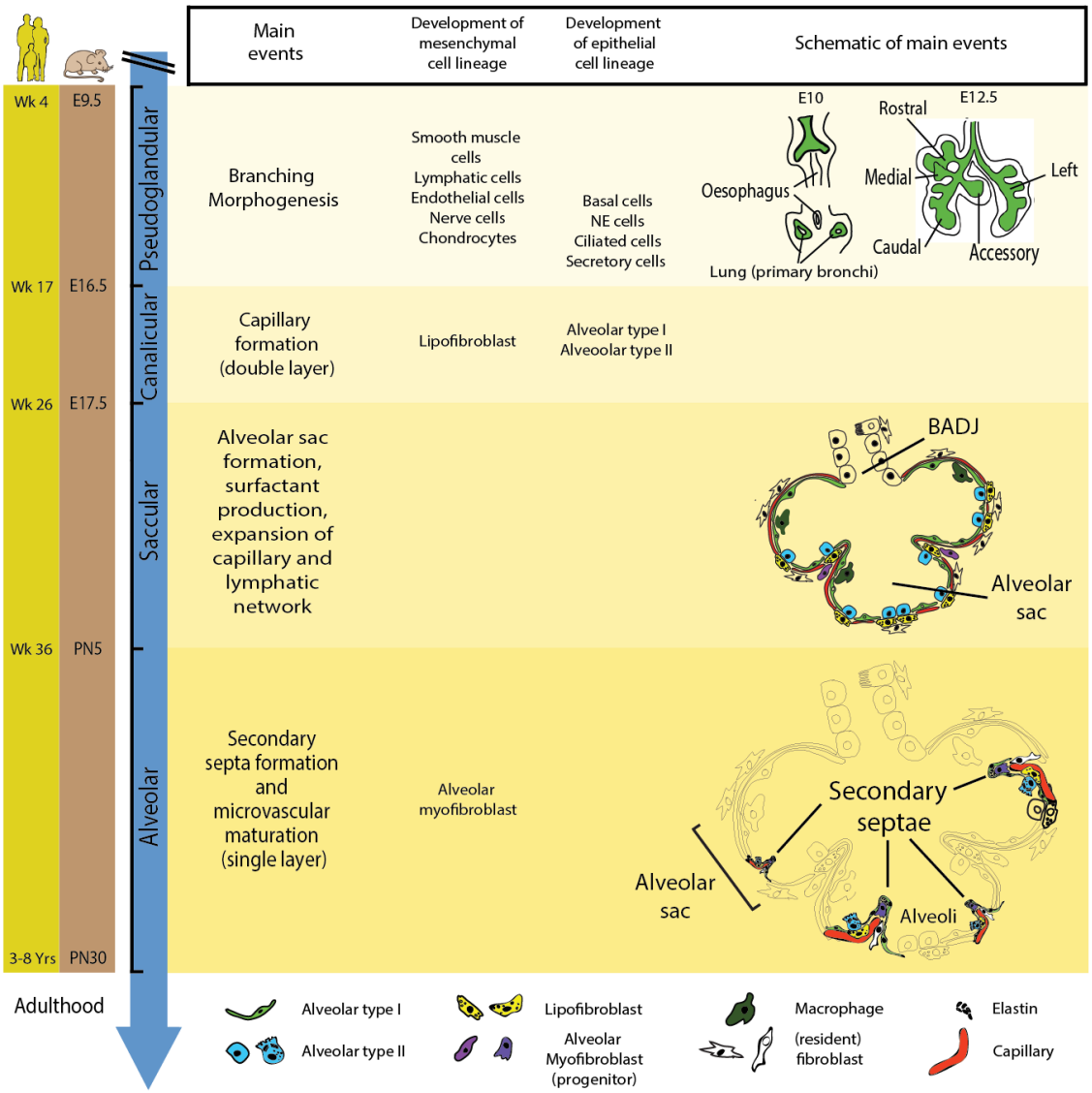

Figure 1: | Timeline and stages of lung development in mice and humans (Chao et al. 2015):

Illustration of the different phases of human and mouse lung development in comparison with a schematic representation of the main events named with the upcoming cell types, which are typical for each developmental stage. The key for the represented cell types is found on the bottom. Moreover, on the left side the time intervals for the particular stage (pseudoglandular, canalicular, saccular, alveolar) are shown in yellow for human and in brown for murine lungs.

Wk: week; E: embryonic; PN: postnatal; BADJ: Bronchioalveolar duct junction;

1.2. The embryonic lung mesenchyme

During lung development, the lung is formed through a sophisticated epithelial-mesenchymal crosstalk that drives lung specification, budding and branching (Chao et al. 2015).

Through a complex signaling network the different compartments induce other processes in the other compartments and vice versa to drive the differentiation of various cell populations. This process is called induction (El Agha und Bellusci 2014).

Signaling molecules like Fibroblast growth factors (Fgf), Wnt (*wingless* and *int*) and Bone morphogenetic proteins (Bmp) are key ligands initiating the pulmonary cell fate and specifying the early lung domain at the ventral foregut endoderm (Hines und Sun 2014).

During the pseudoglandular stage of lung development (around E13.5), the distal lung bud is composed of three morphologically distinguishable layers:

- The epithelium
- The mesenchyme
- The mesothelium

The epithelium forms the inner layer and the mesothelium the outer layer. The mesenchyme (middle layer) can be divided into two domains, the submesothelial mesenchyme (SMM) and the subepithelial mesenchyme (SEM). Progenitors of these two areas give rise to various cell types such as parabronchial smooth muscle cells (PBSMC), vascular smooth muscle cells (VSMC), resident mesenchymal stem cells (MSC), lipofibroblasts, endothelial cells, chondrocytes, nerve cells, alveolar myofibroblasts, lymphatic cells and others (Chao et al. 2015).

1.3. Alveolar lineage formation during lung development

The first multipotent epithelial progenitor cell was detected at the distal tip of the embryonic lung at E10.5 expressing SRY (sex determining region Y)-box 9(Sox9) as well as the inhibitor of differentiation 2 (Id2) (Figure 2). Using a lineage tracing approach (Id2 $^{Cre\text{-}ERT2}$ knock-in mousseline) Rawlins and colleagues showed that Id2+ progenitor cells labeled at the pseudoglandular stage give rise to all the epithelial cell types of the lung (Rawlins et al. 2009).

By labeling the Id2+ cells during the canalicular stage, they marked only the differentiated cells along the alveolar lineage, the AEC I and II cells. These findings suggest that Id2 during the pseudoglandular stage is a marker for the multipotent epithelial progenitor cells, which initially differentiate into bronchiolar progenitors carrying the markers SRY (sex determining region Y)-box 2+ (Sox2+) and alveolar progenitors (Id2+, Sox9+) (Figure 2).

The bronchiolar progenitor cells give rise to club cells, ciliated cells, goblet cells, and neuroendocrine cells. All of which populate the conducting airway epithelium.

The multipotent epithelial progenitor cells give rise to alveolar bipotent progenitors (Id2+, Sox9+, Pdpn+, Sftpc+) during the canalicular stage, which contribute to the population of AEC I and AEC II cells (Treutlein et al. 2014) (Figure 2).

The molecular and cellular mechanisms regulating the differentiation of the different developments are still under research.

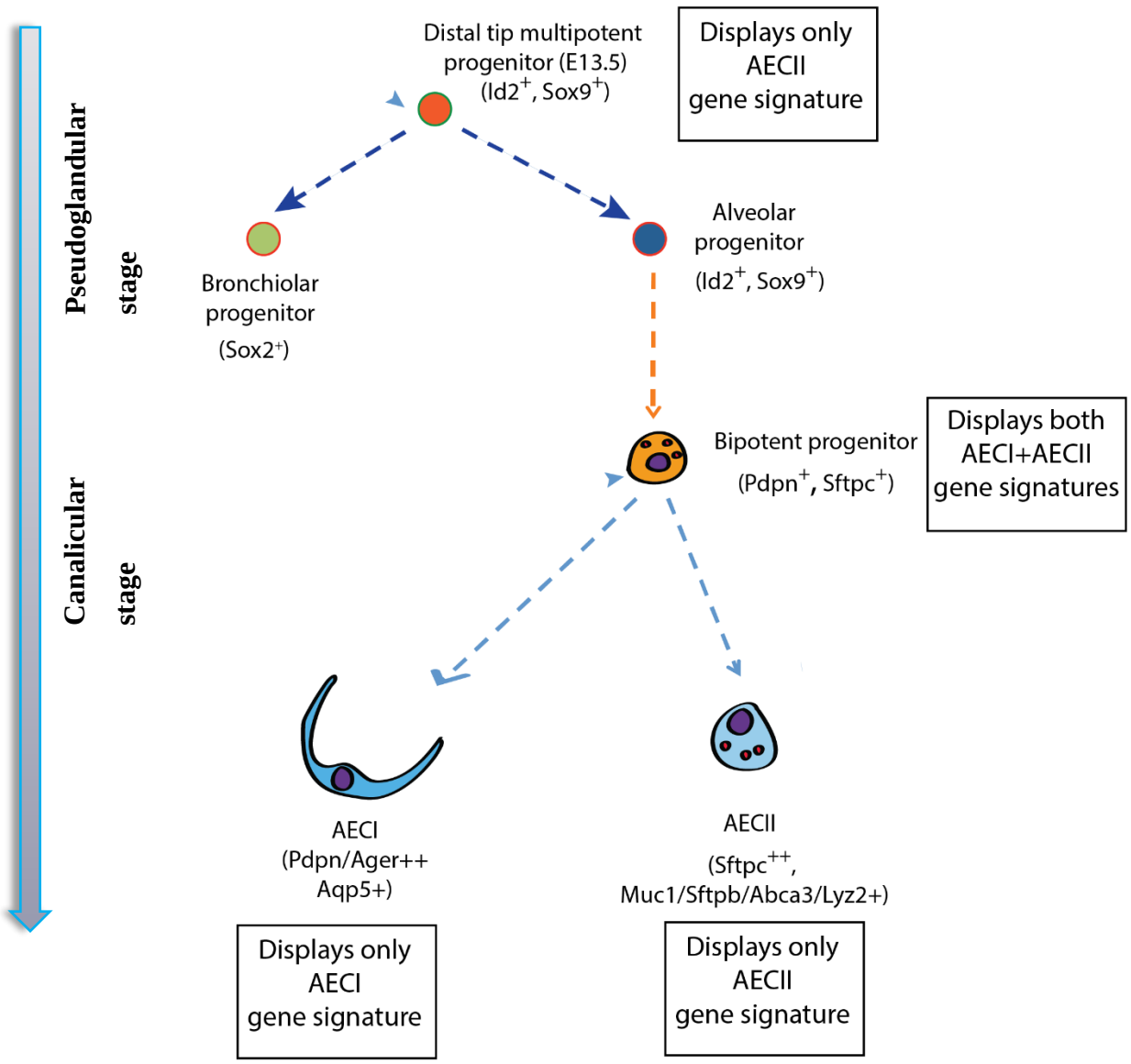

Figure 2: Model for alveolar lineage formation during embryonic lung development (adapted from El Agha et al. 2014).

The multipotent progenitor cells (Id2+, Sox9+) located at the distal tip of the branches give rise to bronchiolar progenitor cells (Sox 9+) and the alveolar progenitor cells (Id2+, Sox9+) during the pseudoglandular stage of embryonic lung development. In turn, the alveolar progenitor cells will give rise to the bipotent progenitor cells during the saccular stage which display both AECI and AECII gene signatures.

Fibroblast growth factors (Fgfs) are a family of growth factors involved in multiple biological processes such as cell division, wound healing, angiogenesis, and they regulate the repair of many organs. (Itoh und Ornitz 2008). Armelin and colleagues reported for the first time in 1970 that pituitary extracts stimulate the growth of fibroblast in a mouse line (Armelin und Armelin 1975). The first Fibroblast growth factors (Fgf1, Fgf2) were isolated from the bovine brain and pituitary (Gospodarowicz et al. 1975; Gospodarowicz and Bialecki 1978). Therefore, the name 'fibroblast growth factor' was given to Fgfs because they could induce the proliferation of fibroblasts. Since then, it has been isolated by several Fgf's.

Fibroblast growth factor 10 (Fgf10) belongs to the fibroblast growth factor family, which is clustered into seven subfamilies and includes 22 members (Itoh and Ornitz 2011a). Fibroblast growth factors exert their wide array of biological effects in an endocrine, paracrine or intracrine manner through seven receptors (FGFR 1b, 1c, 2b, 2c, 3b, 3c and 4). The three domains of each receptor can be divided into an extracellular ligand-biding domain (D1-D3), a transmembrane domain and an intracellular tyrosine kinase domain, which are encoded by four FGFR genes (Szebenyi and Fallon 1999). Fibroblast growth factor receptors get activated in the presence of heparin, heparin sulfate (HS) or other glycosaminoglycan chains. (Ornitz and Leder 1992; Taylor et al. 2005).

This is then leading to the formation of Fgf-Fgfr-HS dimers, which enables the cytoplasmic kinase and activates different intracellular signaling pathways, allowing the transmission of biological responses (Mohammadi et al. 2005).
Ligand and tissue specificity are an essential mechanism for regulating Fgf activity. It is achieved by alternative splicing in immunoglobulin-like domains D2 and D3 and the connecting area in between the two of them (Ornitz und Itoh 2015a).
Genetic deletion of *Fgf10* causes lung agenesis as shown in several studies (Sekine et al. 1999;Bellusci et al. 1997b;Bellusci et al. 1997a).

It was also shown that during the pseudoglandular stage, Fgf10 maintains the undifferentiated status of the SOX9+/ID2+ cells in the distal epithelium (Volckaert et al. 2013; Nyeng et al. 2008).

Fgf10 is one of the genes, which is already expressed in the early pseudoglandular stage of embryonic mouse lung and is absolutely required for initial lung formation. It influences branching morphogenesis and differentiation of the epithelium and

mesenchyme. Fgf10 is expressed in the submesothelial mesenchyme at the distal lung buds (Bellusci et al. 1997b). Fibroblast growth factor receptor 2-IIIb (Fgfr2b) is one of the main receptors of Fgf10, which is located in the distal epithelium cells (Igarashi et al. 1998; El Agha und Bellusci 2014).

1.3.1. The role of Fgf10/Fgfr2b signaling in the formation and maintenance of the alveolar lineage

*Fgf1*0 among others is one of the most important genes of the developing lung from the beginning of organogenesis. It plays a decisive role in controlling epithelial morphogenesis (Chao et al. 2016). The role of Fgf10/Fgfr2b signaling in the formation of the alveolar lineage has been suggested mostly from partial loss or gain of function approaches. Bellusci and colleagues showed in vitro experiments that Fgf10 acts primarily on the epithelium by promoting chemotaxis rather than proliferation (Bellusci et al. 1997b).

Desai and colleagues displayed that postnatally new AEC I cells derive from mature AEC II cells after injury of the alveolar epithelium. This suggested the stem cell function of the AEC II cells after injury (Desai et al. 2014).

Fgf10 is secreted by Lipofibroblasts (LIF), which are located in close proximity to AEC II. It is tempting to speculate that Fgf10 secreted by LIFs is essential for maintaining the AEC II stem cell function (Chao et al. 2016).

Additionally, on its developmental function, Fgf10 is also an important player in the regeneration of the lung after injury. *Fgf10* overexpression demonstrated a protective and therapeutic mechanism in bleomycin-mediated lung injury in mice (Gupte et al. 2009). It is also involved in the regeneration of the bronchial lung epithelium after naphthalene injury (Volckaert et al. 2011). It is also believed that Fgf10 deficiency leads to vasculature defects during normal lung development and during injury (Chao et al. 2019).

Like already mentioned before, the formation of alveoli is initiated by the emergence of the secondary septa and elastin, which is at the apex of the alveolar myofibroblast. Both elastin and alveolar myofibroblasts are critical for the formation of secondary septa showed by the *elastin* knockout mice (Wendel et al. 2000) and *pdgfa* (platelet-derived growth factor A chain) Ko mice (Boström et al. 1996). In both studies are the

alveologenesis significantly reduced or blocked. Ramasamy and colleagues demonstrated that *Fgf10* deficiency mice (expressing only 20 % *Fgf10* compared to WT) had expanded respiratory airways at birth, characterized by the absence of smooth muscle actin myofibroblast (Ramasamy et al. 2007).

The inhibition of Fgfr2b ligands using the soluble *Fgfr2b* approach from E16.5 to E18.5 leads to impaired postnatal alveologenesis, consistent with a role for Fgf10 signaling in the formation of the alveolar myofibroblasts (Hokuto et al. 2003).
A re-expression of *sFgfr2b* blocks also the regeneration process, which signalize that Fgfr2b ligands expressed in the postnatal lung are also critical for the formation of the secondary septa (Perl und Gale 2009). These data indicate that one or several Fgfr2b ligands, in particular Fgf10, are solely responsible for the formation of the alveolar myofibroblasts.

Chao and colleagues demonstrated the role of Fgf10 in an hyperoxia-induced neonatal lung injury in the model of bronchopulmonary dysplasia. They investigated a Fgf10-deficiency in *Fgf10+/-* with a 50% reduction of *Fgf10* versus *Fgf10+/+* (control mice). It was shown that both groups survived under normoxia with no difference in histology. In contrast, all *Fgf10+/-* pups died under hyperoxic conditions (85% O2) after a couple of days after birth while all *Fgf10+/+* pups survive (Chao et al. 2017).

Moreover, a FACS-analysis of the *Fgf10+/-* lungs versus the control groups in normoxia revealed a decrease in AEC II cells over total Epcam-positive cells (general marker for epithelial cells). In isolated AEC II cells from *Fgf10+/-* lungs in gene array analysis would also view a reduction of AEC II transcriptome signatures in contrast to AEC I transcriptome signatures. Such an imbalance is associated with a reduction of surfactant protein B and C expression (Chao et al. 2017).

For targeted investigation, Chao and colleagues used a dominant negative soluble Fgfr2b expression approach (*Rosa26rtTA/+;Tg(tet(O)sFgfr2b)/+* mice), which by ubiquitous and doxycycline-inducible manner, interrupted the Fgfr2b signaling in the postnatal lung development to attenuation the Fgfr2b signaling (Volckaert et al. 2013; Parsa et al. 2010; MacKenzie et al. 2015; Danopoulos et al. 2013).

In the normoxia group they observed no lethality and no structural defects between the two groups. In contrast, with hyperoxia they showed a significant lethality during the

saccular/alveolar stage of lung development. This study suggests that Fgf10 signaling might have a protective ability in hyperoxic lung injury and might mitigate the consequences of bronchopulmonary dysplasia (Chao 2017).

Furthermore, they suggest that Fgf10 has a key role in the differentiation of the bipotent progenitor cells towards the AEC II lineage and a deficiency of Fgf10 also decreased the AEC II cells with their primary function of surfactant production (Chao et al. 2017).

To see the exact effects, we completed the further examination of an inducible and cell specific mouse model to attenuate the Fgfr2b in Sftpc+ cells.

1.4. Pathologies associated with FGF10 dysregulation in human

An interruption of Fibroblast growth factor signaling can lead to various pathologies. A missense mutation in the *FGF10* gene is associated with Aplasia of lacrimal and salivary glands (ALSG) (Scheckenbach et al. 2008). It was also found that mutations in *FGFR2*, *FGFR3* and *FGF10* genes are associated with the autosomal-dominant Lacrimo-auriculo-dento-digital syndrome (LADD). The effects of LADD are common malformation of ears, teeth, fingers, kidney, respiratory system and genitals, and is accompanied with facial dysmorphism, deafness and aplasia of the lacrimal duct (Shams et al. 2007). While these patients initially appear to have normal lung function, that may finally contribute to the development of chronic obstructive pulmonary disease (COPD) later on (Klar et al. 2011). Overexpression of *Fgf10* in the sclera might be associated with an extreme form of myopia (Yoshida et al. 2013).

2. OBJECTIVES

Branching morphogenesis is one of the important process in the developing lung leading to the ramification of a rudimentary tree to a mature organ of overly complex structure, which finally provides gas exchange. However, the exact molecular and cellular bases underlying the formation are still unclear.
Fibroblast Growth Factor 10 (Fgf10) and its receptor fibroblast growth factor receptor 2b (Fgfr2b) play an important role in early lung development. An inactivation of Fgf10/Fgfr2b signaling leads to lung agenesis in mice. (Bellusci et al. 1997a; Sekine et al. 1999).

Jones and colleagues already demonstrated the effect of Fgfr2b inhibition at an early time at E 12.5 showing an arrest in epithelial branching and abnormal cellular adhesion after 9 h (Jones et al. 2018).

To further analyze this pathway at later developmental stages, we used a double transgenic (DTG) approach (mouse line *Rosa26* $^{rtTA/rtTA}$*; Tg(tet(O)sFgfr2b)/+)* to induce the expression of a soluble form of *Fgfr2b* to inactivate Fgfr2b ligands (loss of function) at embryonic day 14.5 and 16.5, which is corresponding to the pseudoglandular respectively canalicular stage in murine lung development.

Furthermore, Chao and colleagues demonstrated the role of Fgf10 signaling in the differentiation of multipotent epithelial progenitors. They showed that Fgf10 deficiency affects the formation of alveolar epithelial cells II (AEC II) quantitatively and qualitatively. Moreover, Fgf10 deficiency is a main reason for lethality in a mouse model of bronchopulmonary dysplasia (BPD) indicating a protective role of Fgf10 in the context of hyperoxic injury (Chao et al. 2017).
For this reason, we applied the triple transgenic mouse line (*Sftpc*$^{CreERT2/+}$*;Tomato*$^{flox/+}$*;Fgfr2b*$^{flox/+}$) to label Sftpc-expressing cells with RFP (red fluorescent protein) and block Fgfr2b signaling in these cells at postnatal day 2 to study the function of Fgfr2b signaling.

With the experiments performed in this study we aim to answer the following two main questions:

1) How does in-vivo ubiquitous attenuation of Fgfr2b signaling during the pseudoglandular (E14.5) and saccular (E16.5) stage of lung development impact the lung on morphological, cellular and gene level?

2) How does cell-specific attenuation of *Sftpc*-expressing cells early postnatally (P2) impact the development of AEC II cells and lung morphology at postnatal day 4 (P4) and postnatal day 17 (P17)?

3. MATERIALS AND METHODS

3.1. Generation and genotyping of mice

3.1.1. Generation

The *Rosa26$^{rtTA/+}$;Tg(tet(o)sFgfr2b)/+* mice (*Gt(ROSA)26SorTm1.1(rtTA,EGFP)Nagy Tg(tet0-sFgfr2b)1Jaw/CHC*) were generated by crossing Rosa26$^{rtTA/+}$ (*Gt(ROSA)26SorTm1.1(rtTA,EGFP)Nagy*) with*Tg(tet(o)sFgfr2b)/+* mice (*Tg(tet0-sFgfr2b))1Jaw/CHC*, obtained from Dr. Jeffrey Whitsett, Cincinnatti, USA) (Hokuto et al. 2003). The mice were kept on the CD1 background for at least 5 generations. Different allelic combinations for the *Rosa26^{rtTA}* and the *Tet(O)sFgfr2b (Tg)* were generated to allow the expression of different levels of soluble *Fgfr2b* following doxycycline (Dox) treatment. All mice were allowed the expression of soluble *Fgfr2b* by administration of doxycycline-containing food (625 mg doxycycline/kg; Altromin Spezialfutter GmbH & Co. KG, Lage, Germany) or via a single intraperitoneal (IP) injection of doxycycline (0.0015 mg per gram body weight) injected to pregnant females.
Both male and female mice were used for the study. C57BL/6 males and females were used to generate wild type pups.

For the mouse triple transgenic model *Stfpc ^{CreERT2}/+ ; Tomato $^{flox/+}$;Fgfr2b $^{flox/+}$* we use a knock-in line where a tamoxifen-inducible Cre recombinase (Cre-ERT2-IRES-YFP) has been inserted. By crossing this line with a *Tomato^{flox}* reporter line, we show that *Sftpc*-positive cells are specifically labeled upon tamoxifen administration in many tissues during postnatal stages.

However, administration of tamoxifen to *Sftpc^{CreERT2}*; *Tomato^{flox}* double transgenic embryos or adult mice results in specific labeling of *Sftpc*-positive cells, which can be lineage-traced temporally and spatially. For the control group we set another litter with *Sftpc$^{CreERT2/+}$;Tomato$^{flox/+}$* transgenic mice. We choose the timepoints P4 and P17 to see changes in the saccular and alveolar stages

3.1.2. Genotyping

Tissues from the tip of the tails of the mice were digested in 200ul Viagen ((Peqlab, 31-102-T, Erlangen, Germany) including 1ul proteinase K (Peqlab, 04-1076, Erlangen, Germany) in 55°C on a shaker overnight, the reaction was stopped in 85°C for 45 min.
To separate the DNA from hairs and bones the isopropanol extraction was done. Solution was centrifuged for 10 min. by 14000 rotation/min. Then the supernatant was removed and isopropanol in 1:1 was added. It was shaken for 10 times slowly and centrifuged again for 10 min. by 14000 rotation/min. The supernatant was removed and 800-900 µl 70% Ethanol was added and vortexed for 1 min. Centrifuge again for 10 min. by 14000 rotation/min. Supernatant was removed and was left for 20 min. by 37°C to dry. 100µl of 0.5xTE Buffer (pH8) was added and mixed for 90 min by 37°C on the Thermomixer.

Genotyping was done by PCR. The different protocols and primer sequences are listed below (Table 1).

Figure 3 represents the expected band-size for Rose26rtTA. For wild type the expected band size is 500 base pairs (bp) and for mutant 1000 bp. For example, sample 4 is positive for both, which means it is heterozygous for *Rosa26*^{rtTA}.

Mouse line	Primer sequence	PCR protocol		
		Step	Temp. (°C)	Time
Rosa26$^{rtTA/+}$	1) GAG TTC TCT GCT GCC TCC TG 2) CGA GGC GGA TAC AAG CAA TA 3) AAG ACC GCG AAG AGT TTG TC	1	94	3min
		2	63	1min
		3	72	1,5min
		4 (repeat Step 2-4 35 times total)	93	1min
		5	72	5min
		6	4	hold
Tg(tet(o)sFgfr 2b)/+	1) GAA GGA GAT CAC GGC TTC C 2) AGA CAG ATG ATA CTT CTG GGA CTG T	1	95	2min
		2	95	5sec
		3	65	5sec
		4 (repeat Step 2-4 35 times total)	72	20sec
		5	72	2min
		6	4	hold

Mouse line	Primer sequence	PCR protocol		
		Step	Temp. (°C)	Time
SPCCre$^{ERT2/+}$	1) CCC AGT CCC TCT CTG AAT TTG 2) GTT TCT ACC GAC CC GTG AAG 3) CAT CGC TCG ACC AGT TTA GTT A	1	94	3min
		2	95	30sec
		3	50	30sec
		4 (repeat Step 2-4 35 times total)	72	1.5min
		5	72	5min
		6	4	hold
Tomato$^{+/+}$	1) TCG TTC CTG TAG GGC ATG G 2) GGC ATT AAA GCA GCG TAT CC 3) CCG AAA ATC TGT GGG AAG TC 4) AAG GGA GCT GCA GTG GAG TA	1	94	3min
		2	94	20sec
		3	61	30sec
		4 (repeat Step 2-4 35 times total)	72	30sec
		5	72	2min
		6	4	hold
Fgfr2b$^{+/+}$	1) CTG CCT GGC TCA CTG TCC 2) CTC AAC AGG CAT GCA AAT GCA AGG TC	1	94	2min
		2	94	30sec
		3	55	30sec
		4 (repeat 2-4 35 times total)	72	1min
		5	4	hold

Table 1: Primer sequences for genotyping of transgenic mouse lines

Mouse line	Expected band size for WT	Expected band size for mutant
Rosa26$^{rtTA/+}$*;Tg(tet(o)sFgfr2b)/+*	Rosa26^{rtTA}: 322bp	Rosa26^{rtTA}: 215bp sFgfr2b: 110bp
SPCCre$^{ERT2/+}$	500bp	1000bp
Tomato$^{+/+}$	297bp	196bp
Fgfr2b$^{+/+}$	380bp	480bp

Table 2. Genotyping and the expected band sizes for wildtype and transgenic mouse lines

Rosa26^{rtTA}

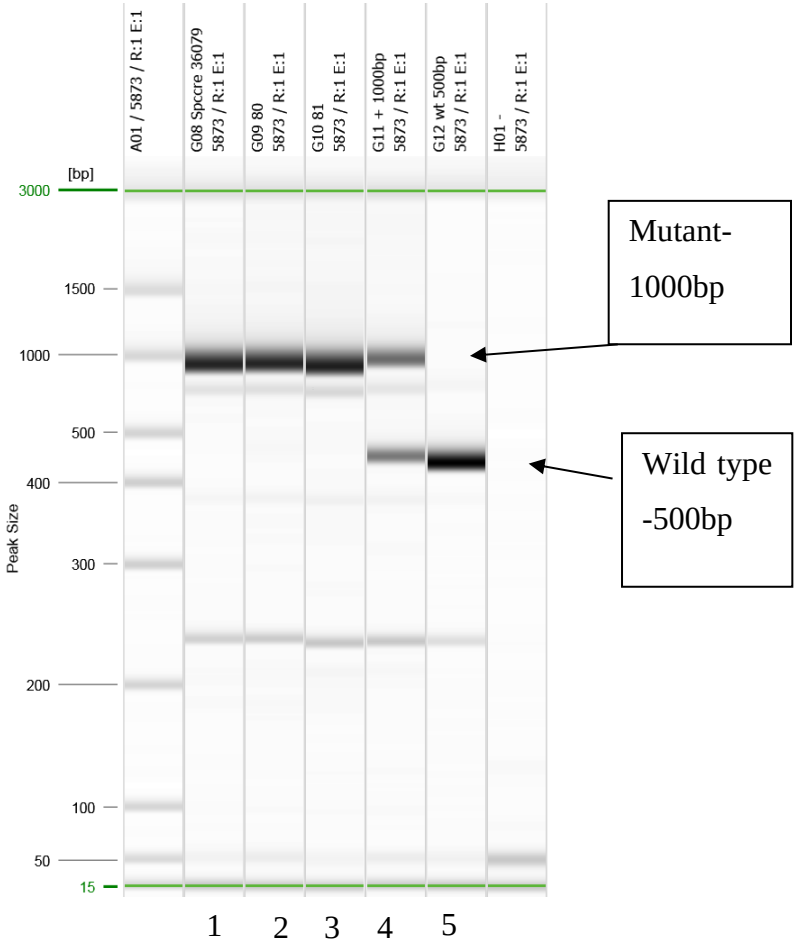

Figure 3: Example for the expected band sizes for *Rosa26^{rtTA}* in wildtype and mutant mice

For wild type the expected band size is 500 base pairs (bp) and for mutant 1000 bp. For example, sample 4 is positive for both, which means it is heterozygous for *Rosa26^{rtTA}*.

Mice 1-3 are homozygous for *Rose26^{rtTA}*, mouse 4 is heterozygous and mouse 5 is a wildtype ; 1-5 mouse samples.

3.2. Lung perfusion and isolation

After the mice were sacrificed with CO2, for safety the neck was broken. Then the lung was flushed with PBS from the right ventricle to remove blood cells from the lung, then perfused through the trachea with a pressure of 20 cm H2O with 5 ml 4% PFA. The

trachea was tied off with a string, and the lung was removed from the body and placed in progressively dehydrated in 30%, 50%, 70%, 95%, 99% ethanol, each for 3 h. Embryonal lungs were only left for 10 min in the different ethanol concentrations. The lungs were incubated in room temperature in xylol until the lungs were transparent then in xylol-wax (1:1) and then in paraffine in the oven by 60°C for 1-2 h to wash the lungs from xylol. Finally, the lungs were embedded with a Leica embedding machine (EG 1150C). the paraffin blocks were kept cold on an ice plate and cut in 4 µm sections with the Leica RM 2235 microtome.

3.3. Gene expression analyses

3.3.1. RNA extraction

The whole embryonic lung was removed and placed in QIAzol lysis reagent (Qiagen GmbH, Hilden, Germany) and frozen in liquid nitrogen for RNA extraction. The lungs were stored by -80°C until RNA extraction could be performed. The frozen lungs were thawed and homogenized in GentleMACs. RNA was isolated using the RNeasy Mini Kit (Qiagen, Hilden, Germany) according to manufacturer's instructions. The samples were nano dropped (NanoDrop 2000c Spectrophometer, PEQLab, Erlangen, Germany) for RNA concentration and purity. Samples were stored at -80°C until reverse transcription was performed (Table 3).

#	Sample ID	User name	Date and Time	Nucleic Acid Conc.	Unit	A260	A280	260/280	260/230	Sample Type	Factor
1	SD47 1-1	Administrator	15.06.2016 16:56:33	1012,2	ng/µl	25,304	12,206	2,07	2,17	RNA	40,00
2	1-2	Administrator	15.06.2016 16:57:38	589,0	ng/µl	14,724	7,103	2,07	1,95	RNA	40,00
3	2-1	Administrator	15.06.2016 16:58:17	737,7	ng/µl	18,443	8,823	2,09	2,13	RNA	40,00
4	2-2	Administrator	15.06.2016 16:58:53	399,9	ng/µl	9,998	4,787	2,09	2,13	RNA	40,00
5	3-1	Administrator	15.06.2016 16:59:22	968,8	ng/µl	24,219	11,692	2,07	1,93	RNA	40,00
6	3-2	Administrator	15.06.2016 16:59:51	448,5	ng/µl	11,211	5,389	2,08	1,89	RNA	40,00
7	4-1	Administrator	15.06.2016 17:00:18	745,3	ng/µl	18,634	9,178	2,03	2,02	RNA	40,00
8	4-2	Administrator	15.06.2016 17:00:46	594,9	ng/µl	14,871	7,193	2,07	2,01	RNA	40,00
9	5-1	Administrator	15.06.2016 17:01:22	868,7	ng/µl	21,717	10,499	2,07	2,06	RNA	40,00
10	5-2	Administrator	15.06.2016 17:01:52	398,7	ng/µl	9,967	4,756	2,10	1,14	RNA	40,00
11	6-1	Administrator	15.06.2016 17:02:25	724,3	ng/µl	18,108	8,889	2,04	1,99	RNA	40,00
12	6-2	Administrator	15.06.2016 17:02:52	445,4	ng/µl	11,135	5,354	2,08	1,70	RNA	40,00
13	7-1	Administrator	15.06.2016 17:03:24	811,5	ng/µl	20,286	9,816	2,07	2,10	RNA	40,00
14	7-2	Administrator	15.06.2016 17:03:53	518,2	ng/µl	12,955	6,128	2,11	2,27	RNA	40,00
15	8-1	Administrator	15.06.2016 17:04:22	996,1	ng/µl	24,904	12,004	2,07	2,02	RNA	40,00
16	8-2	Administrator	15.06.2016 17:04:50	504,1	ng/µl	12,602	6,089	2,07	2,08	RNA	40,00
17	9-1	Administrator	15.06.2016 17:05:20	978,2	ng/µl	24,456	11,786	2,08	2,06	RNA	40,00
18	9-2	Administrator	15.06.2016 17:05:48	585,3	ng/µl	14,632	7,092	2,06	1,81	RNA	40,00
19	10-1	Administrator	15.06.2016 17:06:20	853,2	ng/µl	21,331	10,278	2,08	1,80	RNA	40,00
20	10-2	Administrator	15.06.2016 17:07:24	521,7	ng/µl	13,042	6,298	2,07	1,26	RNA	40,00
21	11-1	Administrator	15.06.2016 17:07:51	797,1	ng/µl	19,927	9,707	2,05	1,85	RNA	40,00
22	11-2	Administrator	15.06.2016 17:08:20	337,7	ng/µl	8,442	4,096	2,06	1,78	RNA	40,00

Table 3: RNA concentration of isolated embryonic lungs

3.3.2. Reverse Transcription and quantitative PCR (RT-qPCR)

RNA samples were kept in -80°C. After thawing, *RNA* was extracted and diluted to the required *RNA* concentration.

RNA was reverse-transcribed (QuantiTect Reverse Transcription Kit, Qiagen, Hilden, Germany). Primers were designed using Roche Applied Sciences Assay Design Tool. All primers were designed to span introns and blasted using NCBI software for specificity. Sybr Green Master Mix (invitrogen/life technologies, 1655057, Germany) was used for RT-PCR with a Roche LightCycler 480 machine.

For genomic *DNA* elimination gDNA wipeout buffer was added to the *RNA* and incubated for 2 min at 42°C. For reverse transcription RT, RT buffer and RT primer mix (QuantiTect Reverse Transcription Kit) were added to the *RNA* and incubated for 50 min at 42°C and for 3 min at 95°C. The *cDNA* resulting out of this procedure can be stored at -20°C.

cDNA was diluted to a concentration of 5 ng/µL. A 96-well plate was used for qPCR. 2 µl of *cDNA* and 18 µl of Mastermix (containing 10 µl Mastermix SybrGreen, 7.2 µl RNase free water, 0.4 µl forward and reverse 10 µM primer respectively) were added to each well. Samples were run in triplicates using Hprt as a reference gene. Mouse primers are listed below (Table 4).

For qPCR, the LightCycler 480 Instrument II (Roche) was used with the following setting:

- Pre-incubation: 55°C for 2 min, 95°C for 5 min.
- Amplification: 95°C for 5 sec, 60°C for 10 sec, 72°C for 10 sec (45 cycles).
- Melting curve: 95°C for 15 sec, 65°C for 1 min, increasing temperature for 0.57°C/s until 97°C.
- Cooling: 40°C for 10 sec.

Gene	Forward primer	Reverse primer
Aqp5	5'-taa cct ggc cgt caa tgc-3'	5'-gcc agc tgg aaa gtc aag at-3'
CC10 (Scgb1a1)	5'-gat cgc cat cac aat cac tg-3'	5'-cag atg tcc gaa gaa gct ga-3'
Hprt	5'-cca cag gac tag aac acc tgc taa-3'	5'-cct aag atg agc gca agt tga a-3'
Spc	5'-ggt cct gat gga gag tcc ac-3'	5'-gat gag aag gcg ttt gag gt-3'

Table 4: Primer sequences for gene expression analyses using RT-qPCR.

3.4. Hematoxylin and eosin (HE) staining

To deparaffinized, the sections were put 3 times in xylol for 5-10 min and then washed with 99%, 95%, 70%, 50% and 30% ethanol for each 2 min. After dipped in MilliQ the sections were stained for Mayer's Hematoxylin solution for 1 – 3 min and washed under running tap water for up to 10min. Slides were looked under the microscope for over and under staining. Slides were then incubated for 2 min in Eosin dye (Richard-Allan Scientific Eosin-Y, 359551, Kalamazoo, MI) and brought back through increasing gradients of ethanol. Slides were put 2 times for 5 min in xylol and then cover slipped with Pertex mounting media.

3.5. Alveolarmorphometry

For alveolar morphometry, the lungs were stained with hematoxylin and eosin (HE) to measure the mean linear intercept (MLI; in µm), mean air space (in %) and mean septal wall thickness (in µm). Total scans from the whole lobe were analyzed using a Leica DM6000B microscope with an automated stage, according to the procedure previously described (McGrath-Morrow et al., 2004; Woyda et al., 2009), which was implemented into the Qwin V3 software (Leica, Wetzlar, Germany) (Figure 4). Horizontal lines (distance 40 µm) were placed across each lung section. The number of times the lines cross alveolar walls was calculated by multiplying the length of the horizontal lines and the number of lines per section then dividing by the number of intercepts. Bronchi and vessels above 50 µm in diameter were excluded prior to the computerized measurement. The air space was determined as the non-parenchymatous non-stained area. The septal wall thickness was measured as the length of the line perpendicularly crossing a septum. From the respective measurements, mean values were calculated.

A

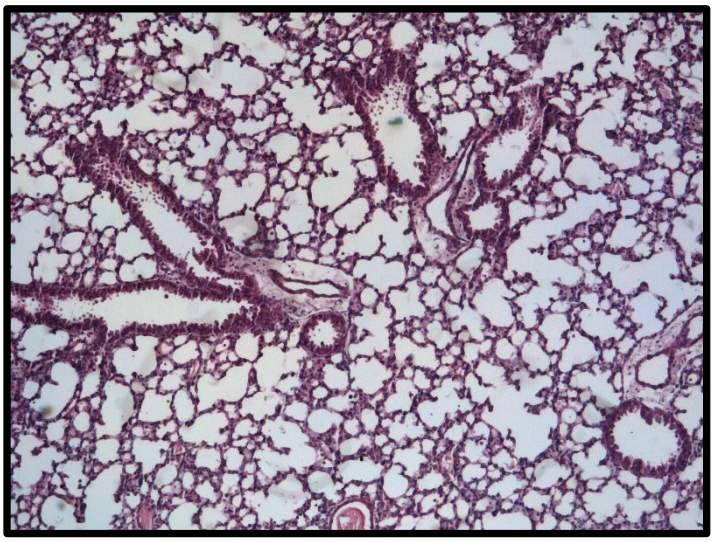

B

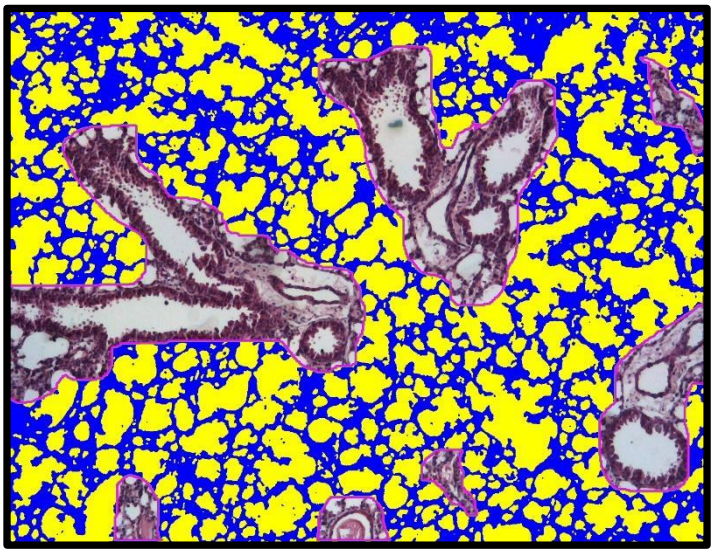

Figure 4: Methodical procedure alveolar morphometry at P17.

Scans of P17 lungs were uploaded into Leica's Qwin V3 software after hematoxylin and eosin staining. (**A**) Lung at P17 before processing with Qwin V3. (**B**) P17 lung after excluding bronchi and vessels. Yellow areas are recognized as air space. Blue areas are recognized as alveolar septa.

3.6. Immunofluorescence staining

Slides were deparaffinized with tree times xylol for 5-10 min and then progressively hydrated in 99%, 95%, 70%, 50% and 30% of ethanol. If antigen retrieval was necessary

it was performed before blocking by placing slides in a staining container and steaming in a pressure cooker with 100mM citrate buffer, pH 6 for 15 min following 30 min cooling on ice and washing three times in TBST (TBS buffer + 0.1% Tween20) for 5 min. Otherwise slides were washed in MilliQ and then 3 times with PBST (PBS buffer + 0.1% Tween20). After slides were blocked with 3% BSA and 0.4% Triton-X in TBS at RT for 1 h, they were incubated with primary antibodies at 4°C overnight. After incubation with antibodies, slides were washed three times in TBST or PBST for 5 min and stained with secondary antibodies at RT for 1 h. The list of the used antibodies is in Table 5. Slides were then washed three times in TBST or PBST for 5 min and mounted with Prolong Gold Anti-fade Reagent with DAPI (Invitrogen).

When antigen retrieval was required for double staining, polyclonal anti-Tomato (anti-RFP) antibodies (Rockland Immunochemicals, 1:220) were used. Apoptosis was detected using DeadEnd Fluorometric TUNEL assay according to manufacturer's instructions (Promega).

The endogenous Tomato signal was detected using the RFP channel. Fluorescent images were acquired using Leica DM5500 B fluorescence microscope and Leica DFC360 FX and DFC420 cameras with Leica Advanced Fluorescence software (2.6.0.7266).

For quantitative analysis, multiple images were used (n > 5). For each experiment, sections from at least 3 independent lungs were analyzed.

Antibodies	**Host/Isotype**	**Supplier**	**Dilution**
Primary Antibodies			
BEK (C-17) Fgfr2	Rabbit	Santa Cruz	1:200
proSPC	Rabbit	Abcam	1:500
RFP	Rabbit	Rockland	1:200
KI67	Mouse	New England Biolabs	1:200
RAGE	Rat	R&D Systems	1:50
Secondary Antibodies			
Alexa Fluor® 488 anti-rat IgG	Goat	Invitrogen	1:500
Alexa Fluor® 594 anti-rabbit	Donkey	Life technologies	1:500
Alexa Fluor® 488 anti-rabbit	Goat	Invitrogen	1:500
Alexa Fluor® 488 anti-mouse	Donkey	Life technologies	1:500

Table 5: The list of primary and secondary antibodies used for immunofluorescence staining.

3.6.1. 5-ethyny1-2´-deoxyuridine (EdU) Staining

Click-iT® EdU Imaging Kit was used to measure the cell ability in embryonic mice. 5 h before harvesting the solution was injected in the maternal mice.

EdU staining was conducted using Click-iT® EdU imaging kit (Invitrogen, Carlsbad, CA) according to the manufacturer's protocol. This protocol is normally intended for use in cell culture but was adapted for histological staining of lung tissue as follows. Slides were deparaffinized with xylol and progressively hydrated in 99%, 95%, 70%, 50% and 30% of ethanol. After washing three times with 3% bovine serum albumin (BSA) in PBS the sections were permeabilized with 0.5% Triton X-100 in PBS for 20 min. The sections were again washed 3 times with 3% BSA in PBS and then incubated with a Click-iT™ reaction cocktail containing Click-iT™ reaction buffer, $CuSO_4$, Alexa Fluor® 555 Azide, and reaction buffer additive for 30 min while protected from light. The sections were washed once more with 3% BSA in PBS. For subsequent DNA staining, sections were washed once with PBS and then incubated with 10 μg/mL Hoechst 33342 for 30 min. The slides were then washed twice with PBS and mounted with Prolong Gold Anti-Fade Reagent with DAPI (Invitrogen). All steps were carried out at room temperature.

3.7. Quantification of immunofluorescence staining

In order to quantify immunofluorescent staining from sections, at least 5 fields of view from each biological sample or treatment group were analyzed. Software ImageJ was used to count the total number of cells (DAPI). The section was then divided into a grid and counted, blindly, to determine the number of stained cells. Percentage of positive cells were calculated accordingly and compared.

To measure the intensity of cell fluorescence of the positive cells, ImageJ (Version 1.8.0-172 NIH, Bethesda, MD, USA) was used. This formula [Integrated Density – (Area of selected cell X Mean fluorescence of background readings)] was used to calculate the corrected total cell fluorescence (CTCF).

3.8. Statistical analysis and figure assembly

Data were analyzed using GraphPad Prism software (GraphPad Software, La Jolla, CA, USA) and presented as average values +/- S.E.M. Statistical analyses were performed using Student's t-test for comparing 2 groups. Results were considered significant if $P < 0.05$. Figures were assembled using Adobe Photoshop CS5 or Adobe Illustrator Ai6.

4. RESULTS

4.1. Effect of blockade of Fgfr2b ligands in embryonic lung

4.1.1. The attenuation of Fgfr2b through sFgfr2b in the pseudoglandular stage leads to less proliferation and more apoptosis

It has been shown that Fgf10/Fgfr2b signaling is crucial for the early lung development (Jones et al. 2018; Bellusci et al. 1997b) but the cellular mechanisms remain unclear.

To further explore the changes on cellular level upon inhibition of Fgfr2b ligands during early lung development, we have used a double transgenic mouse line (*Rosa26$^{rtTA/rtTA}$; tet(O)sFgfr2b)* which allows to attenuate the ligands activity by expressing a dominant negative receptor. After exposure to doxycycline (dox) via food or intraperitoneal (IP) injection, the transactivator rtTA is activated and the soluble Fgfr2b is expressed. This fusion protein binds to Fgfr2b ligands preventing them to interact with their endogenous receptor. This model *(Rosa26$^{rtTA/rtTA}$; tet(O)sFgfr2b)* was validated in many developmental models: In the context of limbs (Danopoulos et al. 2013), mammary glands (Parsa et al. 2008), rodent incisors (Parsa et al. 2010) and gut homeostasis (Al Alam et al. 2015a).

In the first in vivo experiment, we attenuated Fgfr2b signaling from E14.5 to E15.5, corresponding to the pseudoglandular stage. The pregnant females carrying control and experimental embryos were given doxycycline intraperitoneally and doxycycline food from E14.5 to E15.5 (Figure 5A).

Bright field imaging shows a difference at the phenotype between the experimental versus control lungs at E15.5 macroscopically. Examination of the experimental and control lungs apparently revealed an impaired branching of the epithelium with the characteristic elongated distal branches and thicker mesenchyme (Figure 5B).

To find out the proliferation and apoptosis process in the lungs, we use the Click-iT® EdU imaging kit (Invitrogen, Carlsbad, CA) to reveal proliferation process and the DeadEnd Fluorometric TUNEL assay (Promega) to reveal the apoptosis process. Immunofluorescence staining for EdU (Figure 5B) shows a significant decrease of proliferation ($p=0.004;0.005$) both in the epithelium and in the mesenchyme in the

experimental (n=6) (e,g) versus control (n=2) (f,h) lungs. Immunofluorescence staining for TUNEL shows an increase of apoptosis in the mesenchyme in the experimental (j,l) versus control (i,k) group but not in the epithelium (p 0.0027). This was confirmed by quantification (Figure 5C). At the pseudoglandular stage at E15.5. it was possible to distinguish the epithelium and the mesenchyme by their appearance. Because of a sufficient accuracy, an examination using FACS was not carried out.

These results demonstrate that the inhibition of Fgfr2b signaling at E14.5 for 24 h impacts the branching and proliferation. although, much more pronounced and drastic at it was shown by Jones and colleagues after 9 h inhibition (Jones et al. 2018). The primary role of Fgfr2b signaling in proliferation was also confirmed at the 24-h time point.

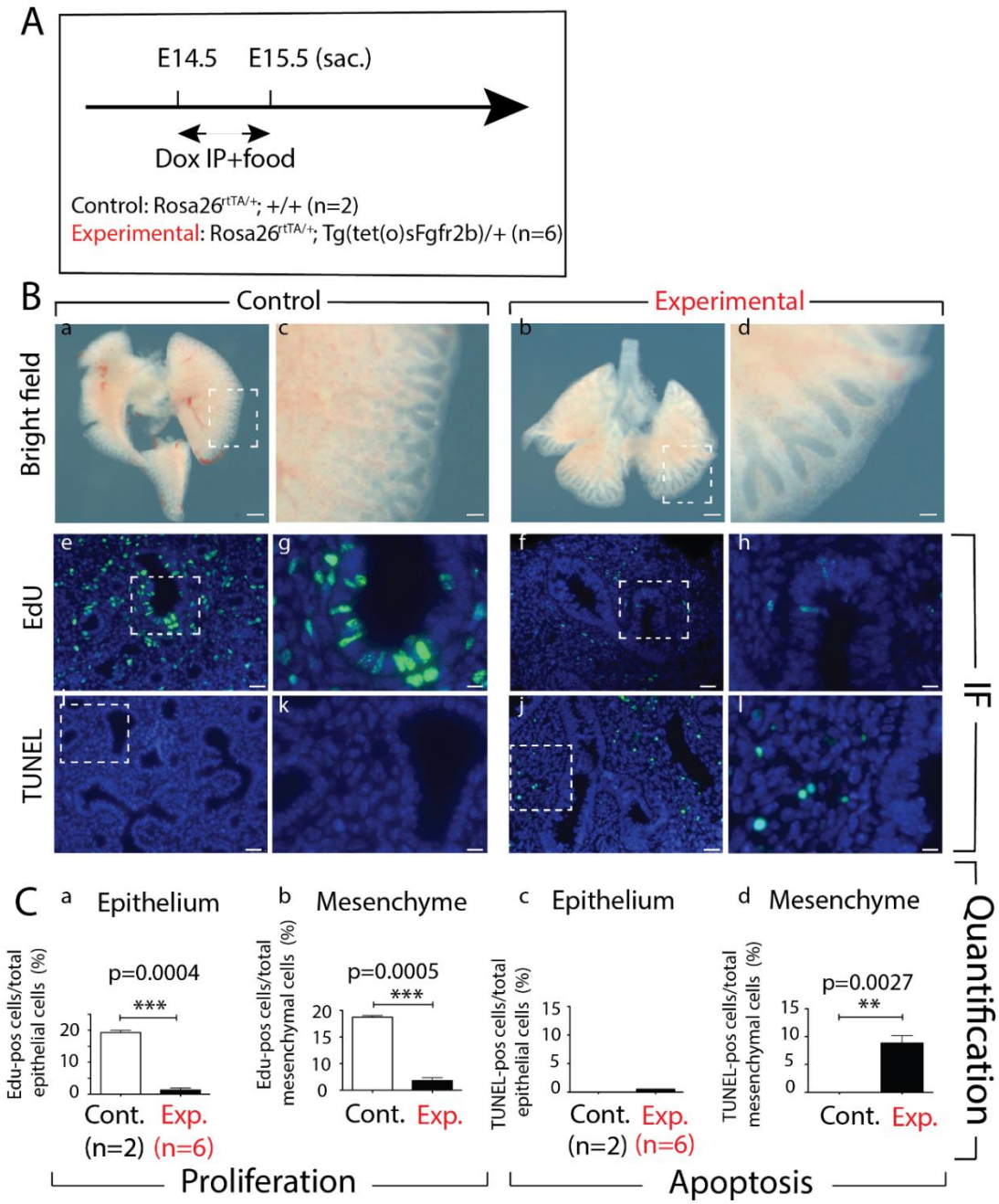

Figure 5: The attenuation of Fgfr2b ligands through sFgfr2b leads to less proliferation and more apoptosis in the pseudoglandular stage.

(**A**) Experimental approach. Pregnant females carrying control and experimental embryos were given doxycycline intraperitoneally and doxycycline food from E14.5 to E15.5. (**B**) Appearance of the control (**a,c**) and experimental (**b,d**) lungs at E15.5. Macroscopically there was a difference between the experimental versus control Lung at E15.5. Note the dilated and less branched branches in the experimental versus control lung. Immunofluorescence staining for Edu showing a significant decrease of proliferation in

the epithelium (**C,a**) as well as in the mesenchyme (**C, b**) in the experimental (n=6) (**e,g**) versus control (n=2) (**f,h**) lungs. Immunofluorescence staining for TUNEL showing an increased apoptosis in the mesenchyme (**C, d**) in the experimental (**j,l**) versus control (**i,k**) group. (**C**) Quantification of Edu-Staining and TUNEL-staining using ImageJ software for epithelium (**a,c**) and mesenchyme (**b,d**).

The Bright field images were kindly provided by Chao Cho-Ming.

Scale bar: (a, b) 750 µm, (c, d) 95 µm, (e, f, i, j) 75 µm, (g, h, k, l) 30 µm.

4.1.2. The attenuation of Fgfr2b through sFgfr2b in the canalicular stage leads to more apoptosis and decrease of surfactant-positive cells

Next, we attenuated Fgfr2b signaling from E16.5 to E17.5 (Figure 6A) to see effects in the canalicular stage of the lung development. In this stage, the lung undergoes further subdivision of the respiratory bronchioles. Here is the first time where a primitive respiratory epithelium is formed by differentiation of distal lung epithelial progenitors. Treutlein and colleagues showed that alveolar epithelial cells type I and II results from alveolar bipotential progenitors (Treutlein et al. 2014).

In this experiment the pregnant females were given again doxycycline intraperitoneally and doxycycline food from E16.5 to E17.5. (Figure 6A). There was a macroscopically difference between the experimental versus control lungs. The experimental lungs were dilated and had less branched branches. That points out that Fgf2b signaling attenuation leads to visible branching defects after 24 h.

In the immunofluorescence staining for apoptosis (TUNEL) we saw an increase of apoptotic cells in the experimental group (n=3) versus control group (n=7) (Figure 6B, i,j,k,l). We did not count the cells in the epithelium and mesenchyme separately as it was exceedingly difficult to distinguish it. Interestingly, we did not find a significant difference in the proliferation staining with EdU (Figure B, e,f,g,h) between the experimental (n=7) versus control (n=3) group. This suggested an attenuation of the Fgfr2b signaling at this stage.

To see the effect of an attenuated Fgfr2b signaling at the Sftpc-positive cells and endothelial cells, we did also an immunofluorescence staining for Sftpc and RAGE. RAGE is a marker for endothelial cells and we wanted to see the effects on the vessels.

The immunofluorescence staining for RAGE showed us obviously no difference between the experimental (n=3) versus control (n=7) lungs (Figure 6B, q,r,s,t).

The immunofluorescence staining for Sftpc showing a decrease Sftpc expression in the experimental (n=3) versus control (n=7) lungs (Figure 6B, m,n,o,p). The quantification of Sftpc-positive cells using ImageJ software shows a significant ($p = 0.005$) decrease in the experimental group versus control group (Figure 6D, c). This experiment clues the impact of attenuation of Fgfr2b through sFgfr2b in the canalicular stage. This suggest that Fgf10/Fgfr2b signaling controls the differentiation balance between AEC I and AEC II cells at the canalicular stage of lung development. In this experiment it was in favor of the AEC II cells.

For a better illustration of the gene level, we did a RT-qPCR with *CC10* (club cells), *Sftpc* (AEC II) and *Aqp5* (AECI) with another litter, where the pregnant females get doxycycline intraperitoneally (Figure 6C). Here, we saw no significant difference between the experimental (n=7) versus control (n=4) lungs. This could be a consequence of the only intraperitoneal doxycycline injection.

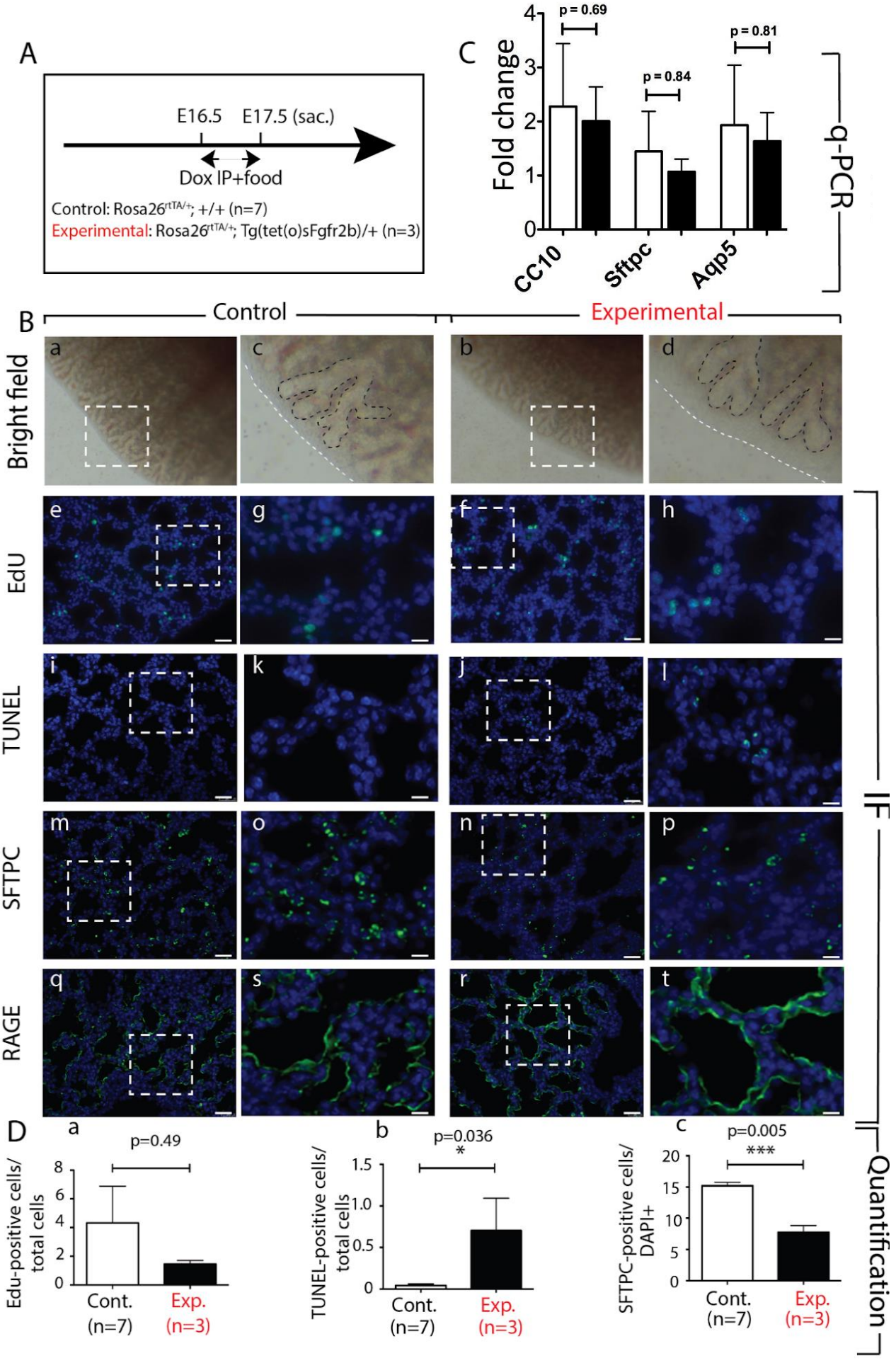
A
E16.5
E17.5 (sac.)
Dox IP+food
Control: Rosa26rtTA/+; +/+ (n=7)
Experimental: Rosa26rtTA/+; Tg(tet(o)sFgfr2b)/+ (n=3)
C
Fold change
p = 0.69
p = 0.84
p = 0.81
CC10
Sftpc
Aqp5
q-PCR
B
Control
Experimental
Bright field
EdU
TUNEL
SFTPC
RAGE
IF
D
a
p=0.49
Edu-positive cells/ total cells
Cont. (n=7)
Exp. (n=3)
b
p=0.036
*
TUNEL-positive cells/ total cells
c
p=0.005
***
SFTPC-positive cells/ DAPI+
Quantification

Figure 6: The attenuation of Fgfr2b through sFgfr2b in E16.5 to E17.5 leads to more apoptosis and less Sftpc expression.

(**A**) Experimental Approach. Pregnant females carrying control and experimental embryos were given doxycycline intraperitoneally and doxycycline food from E16.5 to E17.5. (**B**) Appearance of the control (**a,c**) and experimental (**b,d**) lungs at E18.5. Macroscopically there is a difference between the experimental versus control lungs. Note the dilated and less branched branches in the experimental (**b,d**) versus control (**a,c**) lung. Immunofluorescence staining for EdU showing no significant difference for proliferation between experimental (**f,h**) and control (**e,g**) lungs. Immunofluorescence staining for TUNEL showing an increased apoptosis in the experimental (**j,l**) versus control (**i,k**) lungs. Immunofluorescence staining for SFTPC showing a decreased SFTPC-expression in the experimental (**n,p**) versus control (**m,o**) lungs. Immunofluorescence staining for RAGE showing no significant difference between experimental (**r,t**) and control (**q,s**) lungs. (C) RT-qPCR for *Scgb1a1*, *Sftpc* and *Aqp5* with no significant gene level at E17.5. (**D**) Quantification of the Sftpc-staining was highly significant. Quantification of Edu-Staining (**a**), TUNEL- (**b**) and Sftpc-staining (**c**) using ImageJ software.

The Bright field images were kindly provided by Chao Cho-Ming.

Scale bar: (e,f,i,j,m,n,q,r) 75 µm, (g,h,k,l,o,p,s,t) 30 µm.

4.2. Blockade of Fgfr2b signaling in Sftpc-expressing cells

Chao and colleagues described a qualitatively and quantitatively effect of the formation auf AEC II due to a deficiency of Fgf10 during embryonic lung development (Chao et al. 2017). To see more effects on the AEC II progenitor cells we used *Sftpc*$^{CreERT2/+}$;*Tomato*$^{flox/+}$;*Fgfr2b*$^{flox/+}$ transgenic mice. We tried to mark the ACE II cells with RFP and block the Fgfr2b signaling in these cells. For the control group we set another litter with *Sftpc*$^{CreERT2/+}$;*Tomato*$^{flox/+}$ transgenic mice. We choose the timepoints P4 and P17 to see reactions in the saccular and alveolar stages.

4.2.1. Validation of the Fgfr2b expression at P4

First, we validated the loss of Fgfr2b in our experimental group using Immunofluorescence staining with BEK (Anti-Fgfr2). We separate the experimental group in experimental 1 (heterozygous n=3) and experimental 2 (homozygous n=2) to

clarify the difference (Figure 7A). Mice were given tamoxifen food from P2 to P4 and sacrifice then at P4. We used immunofluorescence staining to show the decrease of BEK (Anti-Fgfr2b) expression in the cells. With ImageJ software we counted the BEK-positive cells relating to all cells (DAPI). We saw a highly significant ($p < 0{,}001$) decrease in the experimental 1, 2 (n=2, n=3) versus control (n=5) group (Figure 7B, g). In the experimental group 2 with the homozygous mice for $Fgfr2b^{f/f}$ they were also quantitatively less Sftpc expression as in the experimental group 1.

For more validation we measure the intensity of BEK in each lung to show also the qualitatively reduction of Fgfr2b in the Sftpc-positive cells and represent them in the Figure 7B, h, i, and j. This formula [Integrated Density – (Area of selected cell X Mean fluorescence of background readings)] was used to calculate the corrected total cell fluorescence (CTCF). The CTCF is an index for pixel intensity that we choose to compare the groups. The cut-off of four was chosen for a better way of illustration.

Here you can also see a decrease of the intensity in the experimental 1 and 2 versus control group. Only 46% of the cells in the control group are under 4 a.u./pixel compared to 69.9% in experimental 1 and 81.3% in experimental 2. Thereby we can assume that the mouse line is working, and we can continue the experiment for more results.

In conclusion, we showed with this experiment that the mouse model reduces the Fgfr2b expression in the Sftpc-positive cells at the time point P4 and P17. From there, we can do further experiments to investigate the role of Fgf10/Fgfr2b in the Sftpc-positive cells during the saccular and alveolar stages.

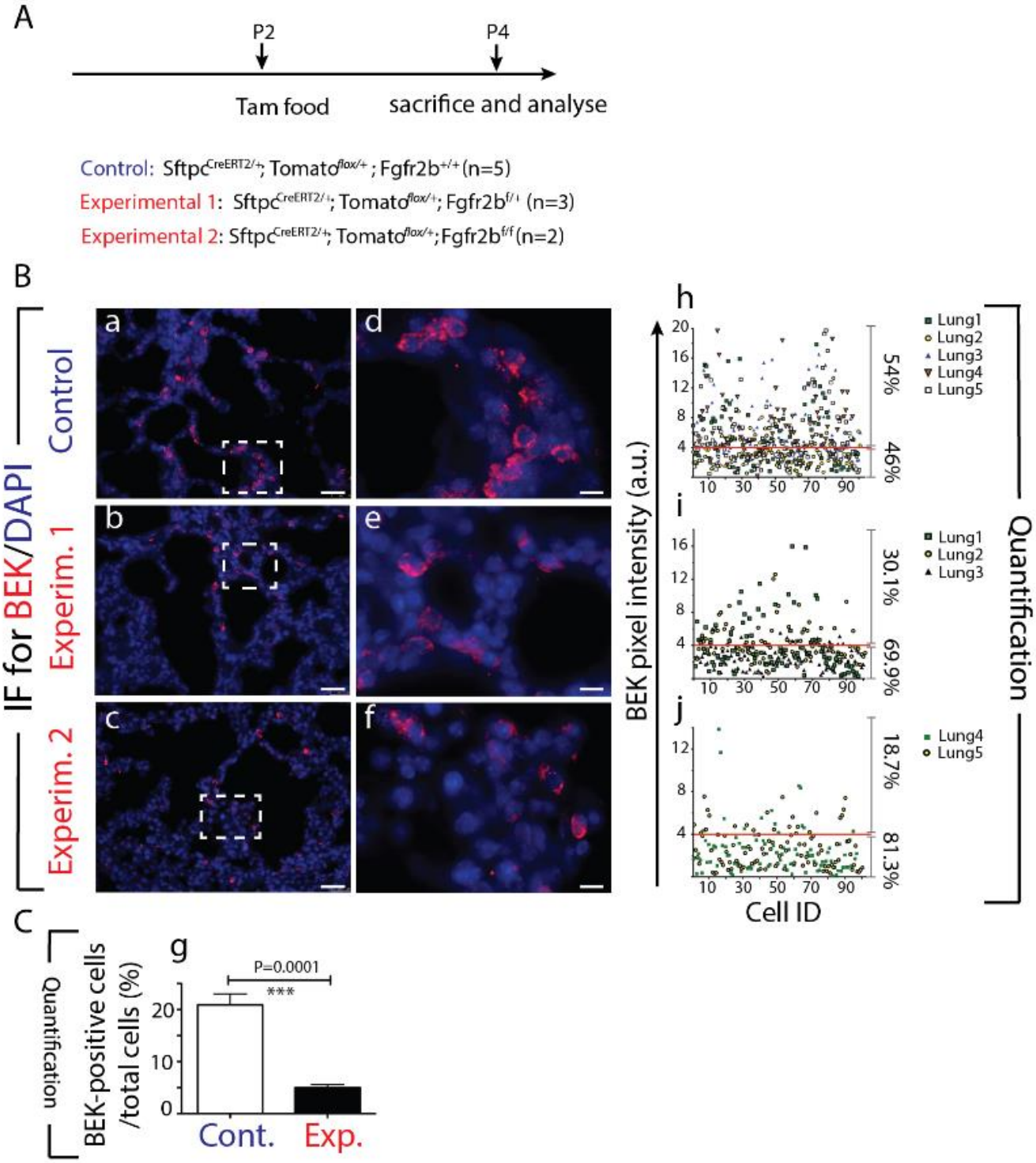
A
P2
P4
Tam food
sacrifice and analyse
Control: Sftpc^CreERT2/+; Tomato^flox/+ ; Fgfr2b^+/+ (n=5)
Experimental 1: Sftpc^CreERT2/+; Tomato^flox/+; Fgfr2b^f/+ (n=3)
Experimental 2: Sftpc^CreERT2/+; Tomato^flox/+; Fgfr2b^f/f (n=2)
B
IF for BEK/DAPI
Control
Experim. 1
Experim. 2
a
b
c
d
e
f
h
i
j
BEK pixel intensity (a.u.)
Cell ID
Lung1
Lung2
Lung3
Lung4
Lung5
54%
46%
30.1%
69.9%
18.7%
81.3%
Quantification
C
Quantification
BEK-positive cells /total cells (%)
g
P=0.0001
***
Cont.
Exp.

Figure 7: Validation of the Fgfr2b expression in Sftpc-expressing cells at P4 upon induced recombination (Fgfr2b^{flox}).

(**A**) Experimental approach. Experimental 1 (n=3) is heterozygous and Experimental 2 (n=2) is homozygous for Fgfr2b. (**B**) Immunofluorescence staining for BEK (Anti-Fgfr2) of control (**a,d**) and experimental (**b,c,e,f**) at P4. Note the highly significant decrease of BEK in the experimental versus control group (**g**). In **B h, i, j** you can see the BEK-pixel intensity for each cell in the different groups The CTCF is an index for pixel intensity that we choose to compare the groups. The cut-off of four was chosen for better way of illustration (Bh,i,j).

Scale bar: (a,b,c) 75 µm, (d,e,f) 30 µm.

4.2.2. *Fgfr2b* deficiency in *Sftpc*-expressing leads to a decrease of Sftpc-expression at P4

The following experiments are designed to identify the onset and the nature of defects in *Fgfr2b* deficiency mouse model in the saccular stage of lung development. We did a double immunofluorescence staining with RFP and Sftpc to detect the effect of Sftpc in the AEC II cells. We saw a significant decrease ($p = 0.016$) of Sftpc in the total Tomato+ cells in the experimental (n=3) versus control group (n=4) (Figure 8C, g). The measurement of the intensity of Sftpc also showed a significant decrease ($p = 0.027$) of the Sftpc-intensity in the experimental versus control lungs (Figure 8C, h). The two experimental groups were done in one group together. For better illustration we represent every group (control, experimental 1 and 2) in a separate graph (Figure 8B, j, k,l). The mark of 2 a.u./pixel was set to show the difference between the groups. Only 9,5% of the cells in the control group are under 2 a.u./pixel compared to 72% in experimental 1 and 71% in experimental 2. To demonstrate the loss of Sftpc after blocking the Fgfr2b signaling, we calculate Tomate+Sftpc-/Tomate+Sftpc+ and show the results in the graph in Figure 8C, i. We had a loss of more than 40% in the experimental group 1 and 2 together compared to the control group. So, we can say that a constitutive Fgfr2b deficiency leads to a decrease of Sftpc-expression in the AEC II progenitor cells.

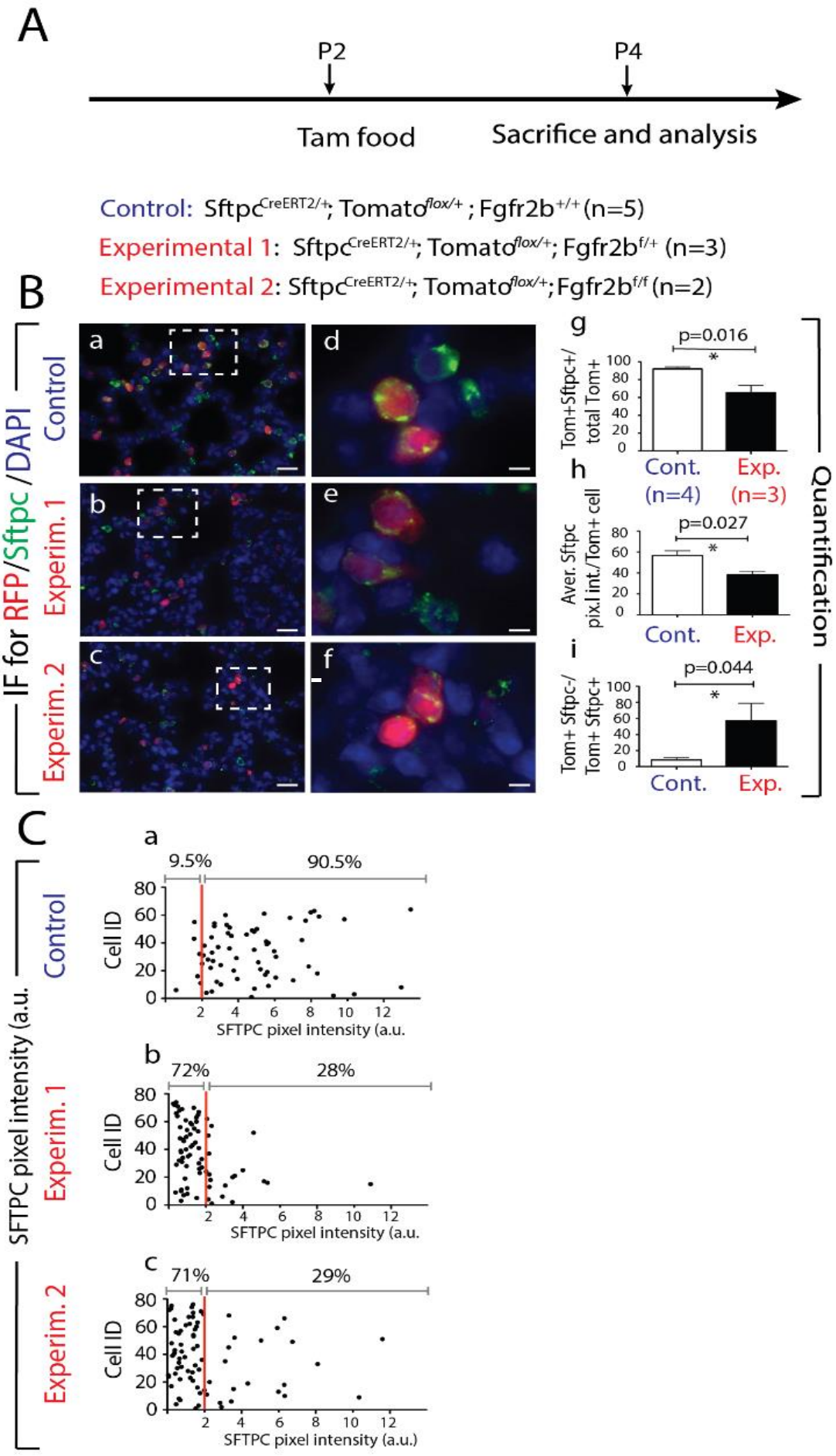
A
P2
P4
Tam food
Sacrifice and analysis
Control: Sftpc CreERT2/+; Tomato flox/+ ; Fgfr2b +/+ (n=5)
Experimental 1: Sftpc CreERT2/+; Tomato flox/+; Fgfr2b f/+ (n=3)
Experimental 2: Sftpc CreERT2/+; Tomato flox/+; Fgfr2b f/f (n=2)
B
IF for RFP/Sftpc /DAPI
Control
Experim. 1
Experim. 2
a
b
c
d
e
f
g
p=0.016
Tom+Sftpc+/ total Tom+
Cont. (n=4)
Exp. (n=3)
h
p=0.027
Aver. Sftpc pixl int./Tom+ cell
Cont.
Exp.
i
p=0.044
Tom+ Sftpc-/ Tom+ Sftpc+
Cont.
Exp.
Quantification
C
SFTPC pixel intensity (a.u.
Control
Experim. 1
Experim. 2
a
9.5%
90.5%
b
72%
28%
c
71%
29%
Cell ID
SFTPC pixel intensity (a.u.)

Figure 8: *Fgfr2b* deficiency in *Sftpc*-expressing cells leads to a decrease of Sftpc-expression at P4.

(A) Experimental approach. The experimental group was splitted in a heterocygot group (n=3) and a homocygot group (n=2) for better illustration **(B)** Immunofluorescence staining for RFP, Sftpc and DAPI showing a significant ($p = 0.016$) decrease of Sftpc in Tomato+ cells in the experimental versus control lungs (**g**). Also note the decrease of the intensity of Sftpc (**h**) in the experimental versus control lungs (Graph: Aver. STFPC pixel int./ Tom + cell). The red cells are Tomato+ cells. (**C**) For better illustration we show the graphs for each group separately (**a,b,c**). Loss of Sfptc after blocking the Fgfr2b signaling (**i**).

Scale bar for Ba, b, c: 75 µm and for Bd, e, f: 30 µm

To illustrate the role of Fgf10/Fgfr2b signaling during the canalicular stage lungs were analyzed at P4 by using H&E staining and alveolar morphometry. Compared to the control group (n =5), lungs in the experimental group 1 and 2 (n=3, n=2) showed a macroscopically decrease in mean linear intercept (MLI) (Figure 9B). There is also a trend of reduction in Airspace (Figure 9B, h). The lungs make the appearance that compactness and not really unfolded. We assume a sacculation defect at the saccular stage.

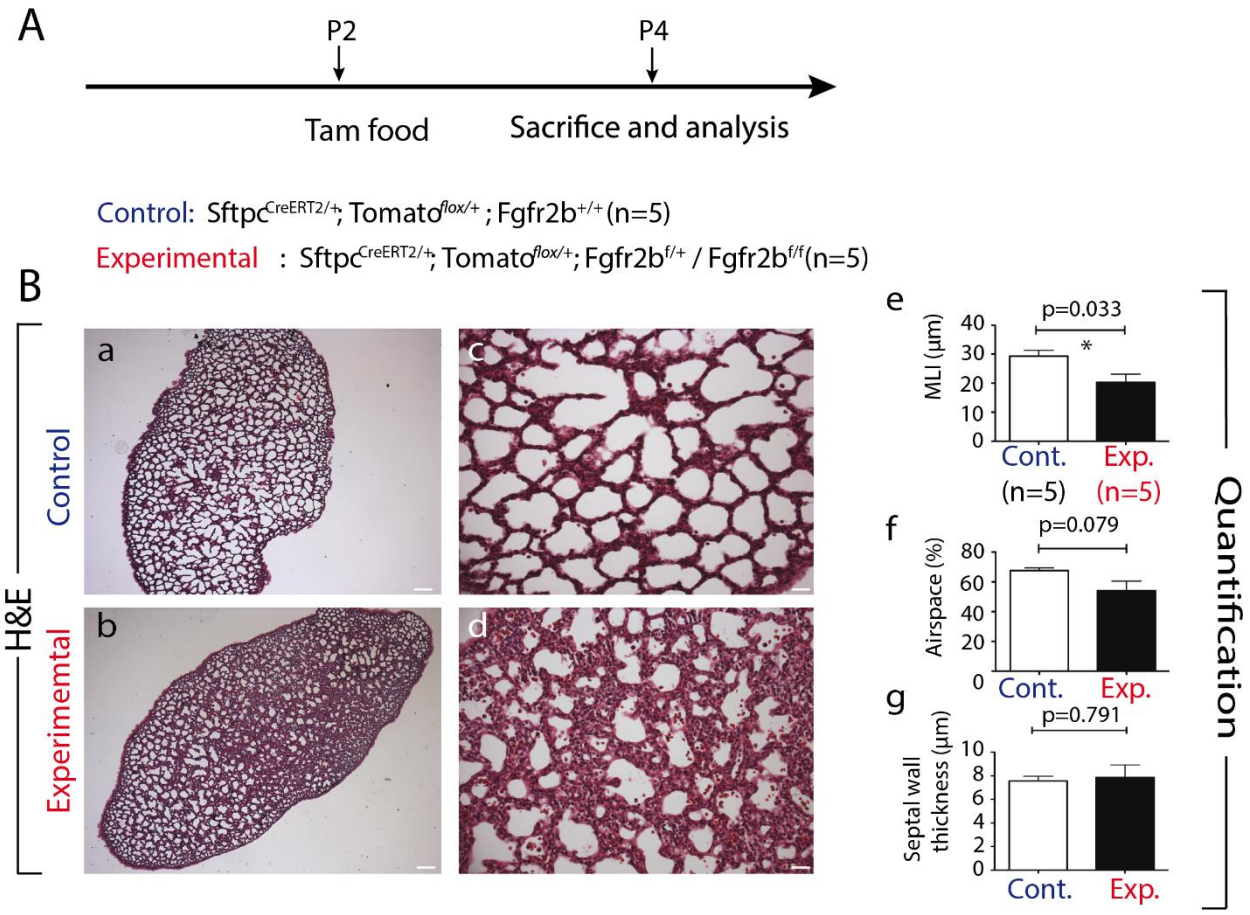

Figure 9: *Fgfr2b* deficiency in *Sftpc*-positive cells leads to a decrease of MLI at P4.

. **(B)** Haematoxylin/eosin staining on control (**a,b**) and experimental (**c,d**) lungs at P4. Corresponding lung morphometric analysis of control and experimental animals. The 2 experimental groups are here together. Note the significant decrease in MLI (**g**) in the experimental group. There was no significant difference in airspace and septal wall thickness between experimental and control group.

Scale bar for a,b 500 µm c,d 50 µm

4.2.3. *Fgfr2b* deficiency in *Sftpc*-expressing cells leads to an increase of septal wall thickness at P17

The following experiments are designed to identify the onset and the nature of defects in *Fgfr2b* deficiency mouse model in the alveolar stage of lung development. We analyzed

lungs at P17 by using H&E staining and alveolar morphometry. Here we saw a significant ($p=0.03$) increase of septal wall thickness in the experimental group ($n=2$) compared to the control group ($n=3$) (Figure 10B). The lungs make the appearance that the development of the alveoli was disturbed. We assume an effect of *Fgfr2b* deficiency to alveolation defect in the alveolar stage at P17. There was no significant difference in airspace and MLI between the experimental and control group. It seems that the *Fgfr2b* deficiency has also an effect in the alveolar stage and leads to less alveolar. We also did immunofluorescence staining with this samples. The results are shown in supplementary data in Figure S1.

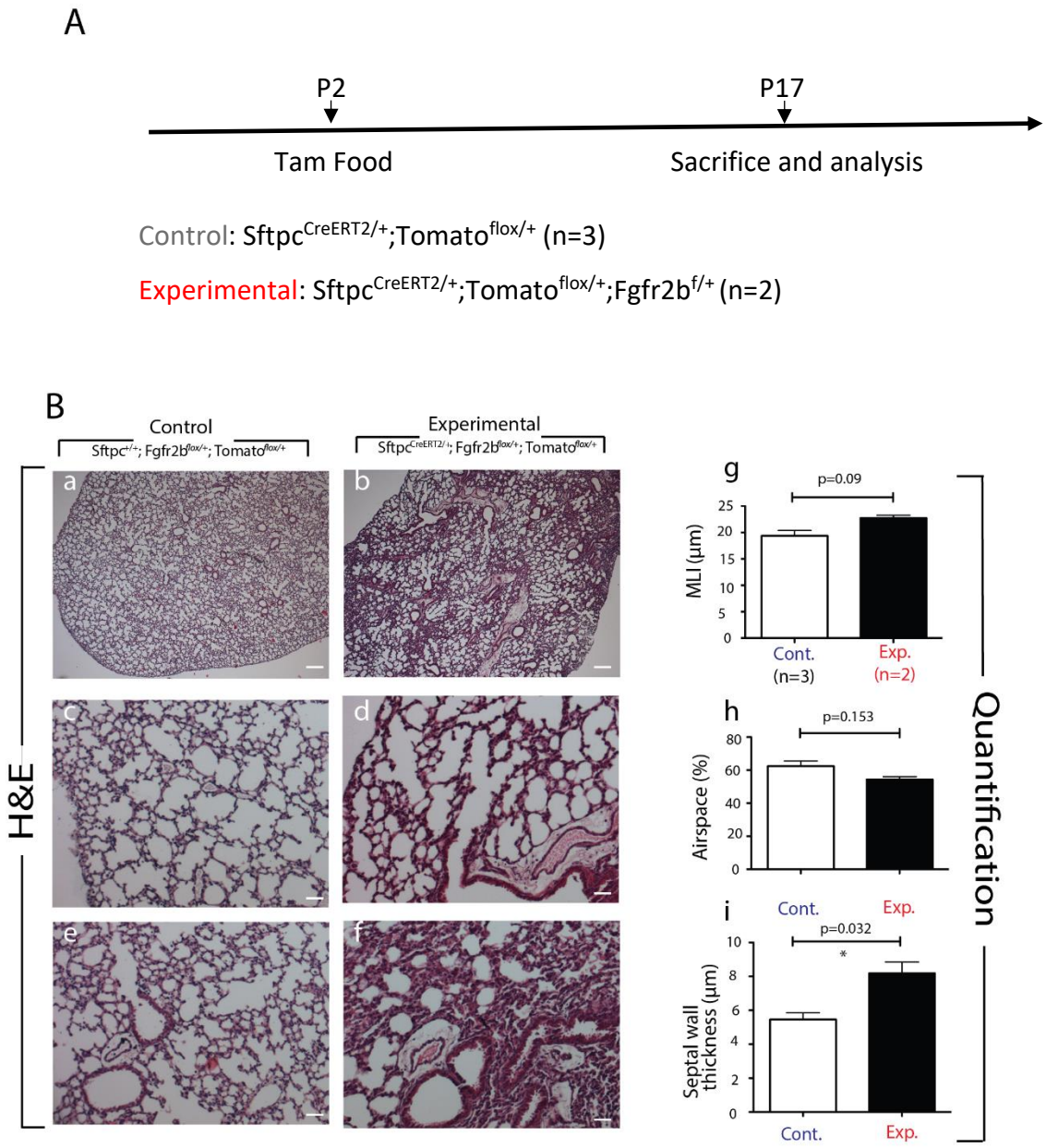

Figure 10: *Fgfr2b* deficiency in Sftpc-expressing cells leads to an increase of septal wall thickness at P17.

(**A**) Experimental approach. Only one of the 3 control lungs are RFP+. (**B**) Hematoxylin/eosin staining of control (**a,c,e**) and experimental (**b,d,f**) lungs at P17. Corresponding lung morphometric analysis. Note the significant increase in septal wall thickness (**i**) in the experimental group.

Scale bar for Ba, b: 500 µm; Bc, d: 250 µm; Bd, e, 50 µm;

4.3. Summary of results

In summary, the questions asked at the beginning of this study (see section 2. Objectives) could be answered as follow:

1) How does in-vivo ubiquitous attenuation of Fgfr2b signaling during the pseudoglandular (E14.5) and saccular (E16.5) stage of lung development impact the lung on morphological, cellular and gene level?

Our data gives evidence on the morphological level an impaired branching of the epithelium with a characteristic elongated distal branches and thicker mesenchyme.

On the cellular level the attenuation of Fgfr2b trough sFgfr2b leads to less proliferation and more apoptosis in the pseudoglandular stage (E14,5.-E15,5) and leads to less *Sftpc*-expression and more apoptosis in the canalicular stage (E16.5-E17.5).

On the gene level we couldn't find any significant differences between the experimental and control groups.

2) How does cell-specific attenuation of *Sftpc*-expressing cells early postnatally (P2) impact the development of AEC II cells and lung morphology at postnatal day 4 (P4) and postnatal day 17 (P17)?

The attenuation of Fgfr2b signaling in AEC II cells leads at the saccular stage of lung development to a decrease of Sftpc-expression in the AEC II cells. Furthermore, morphologically there was also a significant reduction of the MLI, which might represent a sacculation defect.

During the alveolar stage (P17) blockade of Fgfr2b signaling leads an increase of septal wall thickness, which might represent an alveolarization defect.

5. DISCUSSION

5.1. The attenuation of Fgfr2b through sFgfr2b at the pseudoglandular (E14.5) and saccular stage (16.5) of lung development

In this study, we were able to get more insight into the role of Fgf10/Fgfr2b signaling in the early lung development in mice. Using a double transgenic mouse model *(Rosa26$^{rtTA/rtTA}$; tet(O)sFgfr2b)* which allows to attenuate the Fgfr2b ligand activity, we showed the morphological and cellular effects at the pseudoglandular and saccular stage in murine lung development. We found that the attenuation of Fgfr2b through sFgfr2b at pseudoglandular stage (E14.5) leads to less proliferation and more apoptosis. Furthermore, we could demonstrate macroscopically an arrest in epithelial branching with characteristic elongated distal branches and thicker mesenchyme. These results demonstrate that the impacts of inhibiting Fgfr2b in the pseudoglandular stage (E14.5) lead to effects on branching and proliferation of progenitor cell differentiation. Jones and colleagues showed also the similar effect at an earlier time point (E12.5) (Jones et al. 2018). A distinction between epithelium and mesenchyme has been made here by its appearance. A differentiation by FACS would have been better. However, we suggest that the primary biological activity of Fgfr2b signaling shifts from the regulation of branching morphogenesis seen in E12.5 (Jones et al. 2018) to cellular proliferation and differentiation at E14.5.

Next, we attenuated Fgfr2b signaling from E16.5 to E17.5 to see effects at the canalicular stage of the lung development. In this stage, the lung undergoes further subdivision of the respiratory bronchioles. Here is the first time where a primitive respiratory epithelium is formed by differentiation of distal lung epithelial progenitors (Rawlins 2008). This experiment clues the impact of attenuation of Fgfr2b through sFgfr2b in the canalicular stage. This suggests that Fgf10/Fgfr2b signaling controls the differentiation balance between AEC I and AEC II cells at the canalicular stage of lung development in favor of the AEC II cells.

Sftpc-positive cells are in the canalicular stage mostly bipotent alveolar progenitor cells that differentiated to the AEC I and AEC II cells. Treutlein and colleagues showed that alveolar epithelial cells type I and II results from alveolar bipotential progenitors (Treutlein et al. 2014). It was previously thought that the bipotent progenitor cell rises at

approximately E14.5 to the mature AEC I and II. More recently, this model has now been questioned. Frank and colleagues showed with lineage tracing of bipotent progenitors using a dual recombinase transgenic system that these cells do not take part significantly to the AEC I and AEC II cells. (Frank et al. 2019). In return, it was proposed that progenitors specific for the AEC I and ACE II cells are already specified at the early pseudoglandular stages (E13.5) (Frank et al. 2019).

Our results indicate that one of the immediate effects of Fgfr2b signaling at E14.5 is to control the further differentiation of AEC II cells. The AEC I cells are at this short time not affected. However, long-term inhibition of Fgfr2b clearly also affects the AEC I lineage (Jones et al. 2020).

We therefore conclude that at E14.5 Fgfr2b signaling is important for the formation of the AEC I as well as AEC II lineages. Further experiments using specific drivers for AEC I or AEC II progenitor cells should be used to examine the deletion of Fgfr2b and evaluate the impact of Fgfr2b signaling inhibition in these two alveolar epithelial lineages.

The qPCR analyses from *RNA* isolated from the whole lung at E16.5 showed no difference at the different gene expression. This could be explained by a single doxycycline intraperitoneal injection. The tissues, which was used for the immunostaining was injected with doxycycline IP as well as doxycycline food.

5.1.1. *Fgfr2b* deficiency in *Sftpc*-expressing cells leads to a decrease of *Sftpc*-expression and decrease of MLI at P4

Another important aspect of our work is the outcomes of the paper from Chao and colleagues. (Chao et al. 2017). They investigated the impact of Fgf10 deficiency on lung development in a BPD mouse model by using $Fgf10^{+/-}$ mice (50% reduction of Fgf10 expression) compared control mice ($Fgf10^{+/+}$). To see more effects on the AEC II progenitor cells we used a triple transgenic mouse model ($Sftpc^{CreERT2/+};Tomato^{flox/+};Fgfr2b^{flox/+}$). We mark the AEC II cells with RFP and block the Fgfr2b signaling in these cells. For the control group we set another litter with $Sftpc^{CreERT2/+};Tomato^{flox/+}$ transgenic mice. We choose the timepoints P4 and P17 to see reactions in the saccular and alveolar stages.

First, we validate the triple transgenic mouse model with immunofluorescence staining with the antibody BEK. Here we could show a quantitatively decrease of Fgfr2 expression in the Sftpc-positive cells (P=0,0001, Figure 7C).

Our results showed that the blockade of Fgfr2b signaling in AEC II progenitor cells leads at the saccular stage of lung development to a decrease of Sftpc-expression in the AEC II cells. Furthermore, morphologically there was also a significant reduction of the MLI, which seems to be a sacculation defect. During the alveolar stage (P17) it leads to a decrease of septal wall thickness, which seems to an alveolarization defect.

Our results suggest that one of the immediate effects of Fgfr2b signaling at P4 in Sftpc-positive cells is to control the further differentiation of AEC II cells. It seems that the further development of Sftpc-positive cells depends from the presence of Fgfr2b signaling.

Yuan and colleagues demonstrated using single cell RNA sequencing that loss of Fgf10/Fgfr2b signaling in bronchial epithelial cells harms the generation of the alveolar epithelial cells after bleomycin injury. Furthermore, they suggest that a reduction of *Fgf10* compromise alveolar epithelial regeneration by bronchial epithelial stem cells. In summary, their results showed that Fgf10/Fgfr2b signaling drives the alveolar epithelial regeneration by bronchial epithelial cells after acute bleomycin-mediated lung injury (Yuan et al. 2019). For this reason, we assume that the loss of Fgf10/Fgfr2b signaling in AEC II cells leads to impairment of the repair process and regeneration.

In addition, it is also confirmed that the insults to the alveolar epithelium, interfering in a loss of AEC II stem cells or mutations in alveolar epithelial cells that either impair their self-renewal and/or impair their differentiation into AEC I cells, can serve as a trigger of pulmonary fibrosis (Barkauskas and Noble 2014).

We therefore conclude that at P4 and P17 Fgfr2b signaling in *Sftpc*-positive cells are important for the formation of the AEC II lineage. Further studies will have to be run to explain the role of Fgfr2b signaling at different stages (canalicular/saccular/alveolar) of lung development as well as during homeostasis and regeneration/repair after injury.

5.2. Fgf10/Fgfr2b signaling controls the differentiation of the epithelium along the alveolar/AEC II lineage

We described the model for alveolar lineage formation during embryonic lung development already in section 1.3. (Figure 2). Now we add the new investigations about the role of Fgf10/Fgfr2b in figure 11. As mentioned, Fgf10 has previously described to maintain the undifferentiated status of the Sox9/Id2 positive cells which are considered to be multipotent epithelial progenitor cells, in the distal epithelium (Volckaert et al. 2013; Nyeng et al. 2008). Chao and colleagues described that *Fgf10* may play a key role in directing the differentiation of the bipotent progenitor cells towards the AEC II lineage (Chao et al. 2017). Our results confirm the role of Fgf10/Fgfr2b signaling in the pseudoglandular and saccular stage that it is important for the formation of the AEC I as well as AEC II lineages (Chao et al. 2017; Jones et al. 2018; Jones et al. 2020).

Frank and co-workers have shown with lineage tracing of bipotent progenitors using a transgenic double recombinant system that the progenitors specific to the cells AEC I and AEC II are already specified in the first pseudoglandular stages (before E13.5). They suggest that the majority of alveolar epithelial lineages give rise from a unlineage-primed progenitor cell rather than multi-, oligo-, or bilineage progenitor cells (Frank et al. 2019). This represents a paradigm shift. However, further investigations are necessary to confirm these conclusions.

Furthermore, we could show the importance of Fgf10/Fgfr2b signaling in the Sftpc-positive cells. Our outcomes suggest that Fgfr2b deficiency at the saccular and alveolar stage of lung development may play a key role in the further differentiation of the AEC II cells. Moreover, *Fgfr2b* deficiency in Sftpc-positive cells at this stage may also lead to sacculation respectively alveolarization defect.

Jacob and colleagues studied the differentiation of human pluripotent stem cells into functional lung AEC using multicolored fluorescent reporter lines. They showed that differentiating NKX2-1+ lung epithelial progenitor cells can give rise to SFTPC+ cells. In contrast to previous reports of the need of feeder cells for culturing primary adult AEC II cells, “epithelial only” alveolar cells were derived and serialized without the use of mesenchymal co-culture (Jacob et al. 2017).

Furthermore, Ikonomou and colleagues described the genetic program of in vivo murine lung progenitors with RNA-sequencing and computer-based identification of signaling pathways. They also tried to answer the proximity of in vitro progenitors to their counterparts in vivo (Ikonomou et al. 2020). The application of these methods opens up new avenues for the rational and systematic development and improvement of pluripotent stem cells-controlled differentiation protocols and can help to advance future studies of lung development.

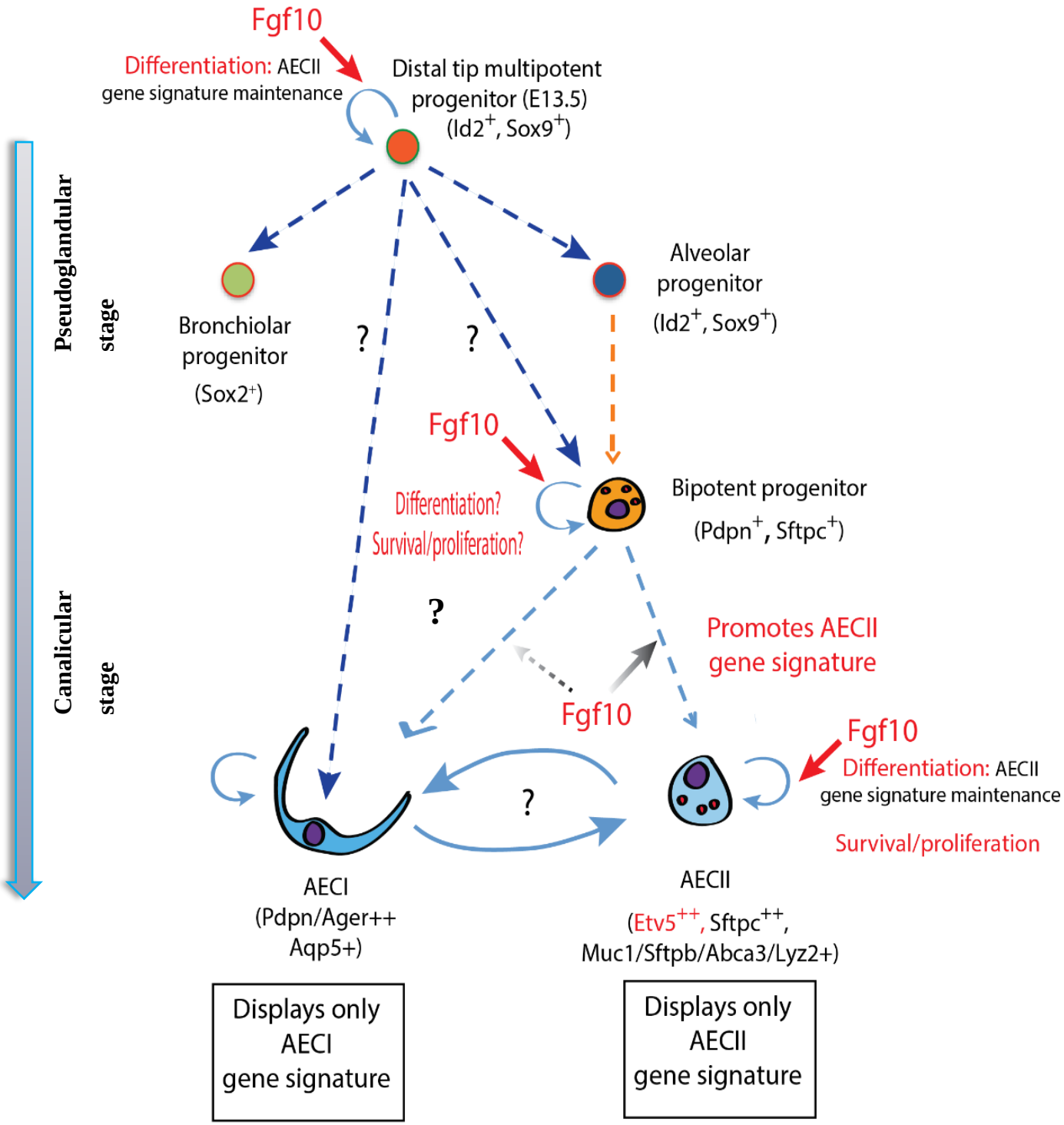
Fgf10
Differentiation: AECII
gene signature maintenance
Distal tip multipotent
progenitor (E13.5)
(Id2+, Sox9+)
Pseudoglandular
stage
Bronchiolar
progenitor
(Sox2+)
?
?
Alveolar
progenitor
(Id2+, Sox9+)
Fgf10
Differentiation?
Survival/proliferation?
Bipotent progenitor
(Pdpn+, Sftpc+)
?
Promotes AECII
gene signature
Fgf10
Canalicular
stage
Fgf10
Differentiation: AECII
gene signature maintenance
Survival/proliferation
?
AECI
(Pdpn/Ager++
Aqp5+)
AECII
(Etv5++, Sftpc++,
Muc1/Sftpb/Abca3/Lyz2+)
Displays only
AECI
gene signature
Displays only
AECII
gene signature

Figure 11: Model for the role of Fgf10/Fgfr2b in alveolar lineage formation during embryonic lung development. (adapted from (El Agha und Bellusci 2014; Chao et al. 2017)

We assume that Fgf10, among others, controls the differentiation of multipotent progenitor cells (Id2+, Sox9+) at the distal end of the branches to alveolar progenitor cells (Id2+, Sox9+) in the pseudoglandular stage of the development of embryonic lungs. Our data suggest that Fgf10/Fgfr2b signaling may orchestrate differentiation and survival/proliferation of this progenitor cell population. Chao and colleagues showed that Fgf10/Fgfr2b signaling favors the differentiation of the progenitor cell towards the AEC II cell. Now our data shows the specific effect of Fgf10/Fgfr2b deficiency on AEC II, which leads to cellular and morphological defects at the saccular and alveolar stage. As Frank and co-workers suggest, the bipotent progenitor cells or the AEC I and AEC II cells could arise directly from the multipotent progenitor cells (Frank et al. 2019).

5.3. Limitation of the study

Although our investigation is based on a mature concept, there are obvious limits to the informative value and interpretability of our results. The limitations are part of each scientific study and will be discussed below.

5.3.1. Differences in lung development in humans and mice and their transferability

The stages of lung development in mammals are generally believed to be similar in species (Schittny 2017). Rodents were widely used to investigate the foundations of lung development, as well as models for human lung diseases and disorders. But the success of translating these findings into the human context is limited (Wong et al. 2019). This is probably in part a consequence of differences in the molecular mechanisms that determine each stage of development when species are compared. For example, Fgf signaling plays one of the most critical roles throughout lung development, and has been studied in depth in mice, with newer human-focused studies (Danopoulos et al. 2019a; Danopoulos et al. 2019b). In mice, Fgf10 and its related receptor Fgfr2b are essential for branching morphogenesis at the pseudoglandular stage of lung developmental, while in humans,

FGF10 seems to be dispensable during this time, becoming more critical in the subsequent canalicular stage (Danopoulos et al. 2019a).

In addition, timing differences between humans and mice are complex, not entirely defined, and may contribute to divergent observations on the role of FGF10 in lung development (Danopoulos et al. 2019a). Further research to clarify the cellular and molecular targets of different FGFs and their receptors in developing human lungs is needed to fill a knowledge gap. This, in turn, will speed up the translational potential of animal studies and open the way for a better therapeutic understanding of the use of individual FGFs in treating human diseases.

5.3.2. Inhibition of Fgf10/Fgfr2b signaling through sFgfr2b

A key limitation of our mouse model for inhibiting Fgf10 signaling during pseudoglandular lung development is that the production of soluble Fgf2b is global, potentially inducing side effects. In addition, soluble Fgfr2b is secreted in the mesenchyme, which potentially inhibits mesenchyme specific Fgf signaling. Al Alam and co-workers already reported that Fgf10 act on the rat lung mesenchyme during the late canalicular/early saccular stage (E19) and influence the differentiation of lipofibroblast progenitors (Al Alam et al. 2015b). Our laboratory already controls the Rosa26$^{rtTA/rtTA}$; tet(O)sFgfr2b mouse model for potential secondary effects by gene array and also by the online database “genepaint,org” (Jones et al. 2018). We are convinced that our global in vivo approach detects the effects of Fgf10 signaling on specific epithelial targets.

5.3.3. Immunofluorescence staining with BEK for Fgfr2b

The immunofluorescence staining for Fgfr2b was performed with the antibody BEK (C17) (Mansukhani et al. 1992) from Santa Cruz, which detected the Fgfr2 isoform. As mentioned in the section 1.3, the Immunoglobulin-like domains II and III, and the linker region between these domains regulates the ligand binding specificity of the four FGFR proteins (Itoh und Ornitz 2011b). Fgfr2 generate two additional major spic variants of immunoglobulin-like domain III, named as IIIb and IIIc (Miki et al. 1992). The splice variants of FGFRb and FGFRc are essential determinants of ligand-binding specificity (Kalinina et al. 2012). The Expression of alternative splice variants of FGFR2 are regulated in a tissue specific manner (Ornitz und Itoh 2015b). Epithelial tissue expresses IIIb splice variants of Fgfr2 and bind ligands that are expressed in mesenchymal tissue such as members of the Fgf7 subfamily (Fgf3, Fgf7, Fgf10 and Fgf 22) (Wu et al. 2010).

By contrast, mesenchymal tissues express IIIc splice variants of Fgfr2, which are often activated by the Fgf4 and Fgf8 subfamilies (MacArthur et al. 1995). Therefore, we are confident that we have chosen the correct antibody to mark the Fgfr2b signaling in the epithelial cells.

5.4. Future perspectives

The understanding of the lung development and alveologenesis process is essential for a lot of lung diseases characterized by lack and/or destruction of alveoli (e.g., BPD, COPD). Therefore, scientists all over the world work hard to disentangle the molecular and cellular bases of lung development in mice before and after birth. Our results help to understand the Fgf10/Fgfr2b signaling in context of lung development and leads to a better view of the morphological and cellular alterations caused by blocking Fgfr2b. In the future, further experiments using specific drivers for AEC I and AEC II progenitor cells should be used to examine the deletion of Fgfr2b and evaluate the impact of Fgfr2b signaling inhibition in these two alveolar epithelial lineages. This will be an invaluable source of information that may be useful to trigger lung regeneration after an injury. This knowledge is essential for the development of novel therapies for the treatment of lung diseases such as BPD and COPD.

6. SUMMARY (ENGLISH)

Fgf10 among others is one of the most important genes of the developing lung from the beginning of organogenesis. It plays a decisive role in controlling epithelial morphogenesis (Chao et al. 2016). It is obvious to assume that Fgf10 might play an important role in both lung development and lung repair after injury.
Jones and colleagues already demonstrated the effect of Fgfr2b inhibition at an early time at E 12.5 showing an arrest in epithelial branching and abnormal cellular adhesion after 9 h (Jones et al. 2018).

To investigate the underlying Fgf10/Fgfr2b signaling mechanism we use a double transgenic mouse mode *(Rosa26$^{rtTA/rtTA}$; tet(O)sFgfr2b)* which allows to attenuate the Fgfr2b activity. Lung morphometry and immunofluorescence staining were performed to identify changes in lung structure.

We found that the attenuation of Fgfr2b through sFgfr2b at pseudoglandular (E14.5) and canalicular (E16.5) stages leads to less proliferation and more apoptosis. Furthermore, we could demonstrate macroscopically an arrest in epithelial branching with characteristic elongated distal branches and thicker mesenchyme. These results demonstrate that the impacts of inhibiting Fgfr2b in the pseudoglandular stage (E14.5) lead to effects on branching and proliferation.

To see also the effect on the ACE II cells we used an inducible and cell specific triple transgenic mouse model *(Sftpc$^{CreERT2/+}$;Tomato$^{flox/+}$;Fgfr2b$^{flox/+}$)*. We mark the AEC II cells with RFP and block the *Fgfr2b* signaling in these cells. We choose the timepoints P4 and P17 to see reactions in the saccular and alveolar stages.

Our results showed that the blockade of Fgfr2b signaling in AEC II progenitor cells leads at the saccular stage P4 to a decrease of Sftpc-expression in the AEC II cells. Therefore, we suggest that one of the immediate effects of Fgfr2b signaling at P4 in Sftpc-positive cells is to control the further differentiation of AEC II cells. It seems that the further development of Sftpc-positive cells depends from the presence of Fgfr2b signaling.

As this study demonstrates, more detailed examinations within each stage of lung development are needed to better understand how Fgf10/Fgfr2b signaling mechanistically operates at the molecular and cellular levels to control lung organogenesis.

New findings and the elaboration of processes of Fgf10/Fgfr2b signaling, which are affected on the biochemical level, may be essential to find potential targets and develop new therapeutic approaches in the future.

5. ZUSAMMENFASSUNG (DEUTSCH)

Von Beginn der Organogenese ist Fgf10 eines der wichtigsten Gene für die Lungenentwicklung. Es spielt eine entscheidende Rolle bei der Kontrolle der epithelialen Morphogenese (Chao et al. 2016). Durch die aktuellen Studienlage ist es anzunehmen, dass Fgf10 sowohl bei der Lungenentwicklung als auch bei der Lungenreparatur nach einer Schädigung eine wichtige Rolle spielen könnte.

Um den zugrunde liegenden Fgf10/Fgfr2b-Signalmechanismus zu untersuchen, verwenden wir einen doppelten transgenen Mausmodus *(Rosa26$^{rtTA/rtTA}$; tet(O)sFgfr2b)*, der es ermöglicht, die Fgfr2b-Aktivität abzuschwächen. Lungenmorphometrie und Immunhistochemie wurden durchgeführt, um Veränderungen in der Lungenstruktur zu identifizieren. Wir fanden heraus, dass die Abschwächung von Fgf10 durch sFgfr2b in pseudoglandulären (E14.5) und kanalikulären (E16.5) Stadium der Lungenentwicklung zu weniger Proliferation und mehr Apoptose führt. Darüber hinaus konnten wir makroskopisch einen Stillstand der epithelialen Verzweigung mit charakteristischen länglichen distalen Ästen und dickerem Mesenchym nachweisen. Diese Ergebnisse zeigen, dass die Hemmung von *Fgfr2b* im pseudoglandulären Stadium (E14.5) zu Auswirkungen auf die Verzweigung der Bronchien und Proliferation führen.

Um auch die Wirkung auf die AEC II-Vorläuferzellen zu sehen, verwendeten wir ein induzierbares und zellspezifisches dreifach transgenes Mausmodell *(Sftpc$^{CreERT2/+}$;Tomato$^{flox/+}$;Fgfr2b$^{flox/+}$).* Wir markieren die AEC II-Zellen mit RFP und blockieren die Fgfr2b-Signalübertragung in diesen Zellen. Wir wählten die Zeitpunkte P4 und P17, um Reaktionen im sakulären und alveolären Stadium zu sehen.

Unsere Ergebnisse zeigten, dass die Blockade der Fgfr2b-Signalübertragung in AEC II-Vorläuferzellen im sakulären Stadium (P4) zu einer Abnahme der Sftpc-Expression in den AEC II-Zellen führten. Daher gehen wir davon aus, dass einer der unmittelbaren Auswirkungen der Fgfr2b-Signalübertragung zum Zeitpunkt P4 in Sftpc-positive Zellen ist die Steuerung der weiteren Differenzierung von AEC II-Zellen. Es scheint, dass die weitere Entwicklung von Sftpc-positiven Zellen vom Vorhandensein von Fgf10/Fgfr2b-Signalmechanismus abhängt.

Wie diese Studie zeigt, sind detailliertere Untersuchungen in jedem Stadium der Lungenentwicklung erforderlich, um besser zu verstehen, wie die Fgf10/Fgfr2b-

Signalübertragung auf molekularer und zellulärer Ebene funktioniert, um die Lungenorganogenese zu steuern.

Neue Erkenntnisse und die Erarbeitung von Prozessen der Fgf10/Fgfr2b-Signalübertragung, die auf biochemischer Ebene beeinflusst werden, könnten wesentlich sein, um potenzielle Ziele zu finden und in Zukunft neue therapeutische Ansätze zu entwickeln.

7. REFERENCES

Al Alam, Denise; **Danopoulos**, Soula; Schall, Kathy; Sala, Frederic G.; Almohazey, Dana; Fernandez, G. Esteban et al. (2015a): Fibroblast growth factor 10 alters the balance between goblet and Paneth cells in the adult mouse small intestine. In: *American Journal of Physiology - Gastrointestinal and Liver Physiology* 308 (8), G678-90. DOI: 10.1152/ajpgi.00158.2014.

Al Alam, Denise; **El Agha**, Elie; Sakurai, Reiko; Kheirollahi, Vahid; Moiseenko, Alena; Danopoulos, Soula et al. (2015b): Evidence for the involvement of fibroblast growth factor 10 in lipofibroblast formation during embryonic lung development. In: *Development* 142 (23), S. 4139–4150. DOI: 10.1242/dev.109173.

Armelin, H. A.; **Armelin**, M. C. (1975): Regulation of fibroblast growth in culture. In: *Biochemical and biophysical research communications* 62 (2), S. 260–267. DOI: 10.1016/s0006-291x(75)80132-x.

Baraldi, Eugenio; **Filippone**, Marco (2007): Chronic lung disease after premature birth. In: *The New England journal of medicine* 357 (19), S. 1946–1955. DOI: 10.1056/NEJMra067279.

Barkauskas, Christina E.; **Noble**, Paul W. (2014): Cellular mechanisms of tissue fibrosis. 7. New insights into the cellular mechanisms of pulmonary fibrosis. In: *American journal of physiology. Cell physiology* 306 (11), C987-96. DOI: 10.1152/ajpcell.00321.2013.

Bellusci, S.; **Furuta**, Y.; Rush, M. G.; Henderson, R.; Winnier, G.; Hogan, B. L. (1997a): Involvement of Sonic hedgehog (Shh) in mouse embryonic lung growth and morphogenesis. In: *Development (Cambridge, England)* 124 (1), S. 53–63.

Bellusci, S.; **Grindley**, J.; Emoto, H.; Itoh, N.; Hogan, B. L. (1997b): Fibroblast growth factor 10 (FGF10) and branching morphogenesis in the embryonic mouse lung. In: *Development (Cambridge, England)* 124 (23), S. 4867–4878.

Benjamin, John T.; **Smith**, Rebekah J.; Halloran, Brian A.; Day, Timothy J.; Kelly, David R.; Prince, Lawrence S. (2007): FGF-10 is decreased in bronchopulmonary dysplasia and suppressed by Toll-like receptor activation. In: *American journal of physiology. Lung cellular and molecular physiology* 292 (2), L550-8. DOI: 10.1152/ajplung.00329.2006.

Bhandari, Anita; **Bhandari**, Vineet (2009): Pitfalls, problems, and progress in bronchopulmonary dysplasia. In: *Pediatrics* 123 (6), S. 1562–1573. DOI: 10.1542/peds.2008-1962.

Boström, H.; **Willetts**, K.; Pekny, M.; Levéen, P.; Lindahl, P.; Hedstrand, H. et al. (1996): PDGF-A signaling is a critical event in lung alveolar myofibroblast development and alveogenesis. In: *Cell* 85 (6), S. 863–873. DOI: 10.1016/s0092-8674(00)81270-2.

Chang, Daniel R.; **Martinez Alanis**, Denise; Miller, Rachel K.; Ji, Hong; Akiyama, Haruhiko; McCrea, Pierre D.; Chen, Jichao (2013): Lung epithelial branching program antagonizes alveolar differentiation. In: *Proceedings of the National Academy of Sciences* 110 (45), S. 18042–18051. DOI: 10.1073/pnas.1311760110.

Chao, Cho-Ming; **Carraro**, Gianni; Rako, Zvonimir A.; Kolck, Johannes; Sedighi, Jamschid; Zimmermann, Volker et al. (2020): Failure to Down-Regulate miR-154 Expression in Early Postnatal Mouse Lung Epithelium Suppresses Alveologenesis, with Changes in Tgf-β Signaling Similar to those Induced by Exposure to Hyperoxia. In: *Cells* 9 (4), S. 859. DOI: 10.3390/cells9040859.

Chao, Cho-Ming; **El Agha**, Elie; Tiozzo, Caterina; Minoo, Parviz; Bellusci, Saverio (2015): A breath of fresh air on the mesenchyme: impact of impaired mesenchymal development on the pathogenesis of bronchopulmonary dysplasia. In: *Frontiers in Medicine* 2, S. 27. DOI: 10.3389/fmed.2015.00027.

Chao, Cho-Ming; **Moiseenko**, Alena; Kosanovic, Djuro; Rivetti, Stefano; El Agha, Elie; Wilhelm, Jochen et al. (2019): Impact of Fgf10 deficiency on pulmonary vasculature formation in a mouse model of bronchopulmonary dysplasia. In: *Human Molecular Genetics* 28 (9), S. 1429–1444. DOI: 10.1093/hmg/ddy439.

Chao, Cho-Ming; **Moiseenko**, Alena; Zimmer, Klaus-Peter; Bellusci, Saverio (2016): Alveologenesis. Key cellular players and fibroblast growth factor 10 signaling. In: *Molecular and cellular pediatrics* 3 (1), S. 17. DOI: 10.1186/s40348-016-0045-7.

Chao, Cho-Ming; **Yahya**, Faady; Moiseenko, Alena; Tiozzo, Caterina; Shrestha, Amit; Ahmadvand, Negah et al. (2017a): Fgf10 deficiency is causative for lethality in a mouse model of bronchopulmonary dysplasia. In: *The Journal of pathology* 241 (1), S. 91–103. DOI: 10.1002/path.4834.

Coalson, Jacqueline J. (2003): Pathology of new bronchopulmonary dysplasia. In: *Seminars in Neonatology* 8 (1), S. 73–81. DOI: 10.1016/S1084-2756(02)00193-8.

Danopoulos, Soula; **Parsa**, Sara; Al Alam, Denise; Tabatabai, Reza; Baptista, Sheryl; Tiozzo, Caterina et al. (2013): Transient Inhibition of FGFR2b-ligands signaling leads to irreversible loss of cellular β-catenin organization and signaling in AER during mouse limb development. In: *PLoS ONE* 8 (10), e76248. DOI: 10.1371/journal.pone.0076248.

Danopoulos, Soula; **Shiosaki**, Jessica; Al Alam, Denise (2019a): FGF Signaling in Lung Development and Disease: Human Versus Mouse. In: *Frontiers in Genetics* 10, S. 170. DOI: 10.3389/fgene.2019.00170.

Danopoulos, Soula; **Thornton**, Matthew E.; Grubbs, Brendan H.; Frey, Mark R.; Warburton, David; Bellusci, Saverio; Al Alam, Denise (2019b): Discordant roles for FGF ligands in lung branching morphogenesis between human and mouse. In: *The Journal of pathology* 247 (2), S. 254–265. DOI: 10.1002/path.5188.

Desai, Tushar J.; **Brownfield**, Douglas G.; Krasnow, Mark A. (2014): Alveolar progenitor and stem cells in lung development, renewal and cancer. In: *Nature* 507 (7491), S. 190–194. DOI: 10.1038/nature12930.

El Agha, Elie; **Bellusci**, Saverio (2014): Walking along the Fibroblast Growth Factor 10 Route: A Key Pathway to Understand the Control and Regulation of Epithelial and Mesenchymal Cell-Lineage Formation during Lung Development and Repair after Injury. In: *Scientifica* 2014, S. 538379. DOI: 10.1155/2014/538379.

Frank, David B.; **Penkala**, Ian J.; Zepp, Jarod A.; Sivakumar, Aravind; Linares-Saldana, Ricardo; Zacharias, William J. et al. (2019): Early lineage specification defines alveolar epithelial ontogeny in the murine lung. In: *Proceedings of the National Academy of Sciences* 116 (10), S. 4362–4371. DOI: 10.1073/pnas.1813952116.

Gospodarowicz, D.; **Bialecki**, H. (1978): The effects of the epidermal and fibroblast growth factors on the replicative lifespan of cultured bovine granulosa cells. In: *Endocrinology* 103 (3), S. 854–865. DOI: 10.1210/endo-103-3-854.

Gospodarowicz, D.; **Rudland**, P.; Lindstrom, J.; Benirschke, K. (1975): Fibroblast growth factor: its localization, purification, mode of action, and physiological

significance. In: *Advances in metabolic disorders* 8, S. 301–335. DOI: 10.1016/b978-0-12-027308-9.50026-3.

Gupte, Varsha V.; **Ramasamy**, Suresh K.; Reddy, Raghava; Lee, Jooeun; Weinreb, Paul H.; Violette, Shelia M. et al. (2009): Overexpression of Fibroblast Growth Factor-10 during Both Inflammatory and Fibrotic Phases Attenuates Bleomycin-induced Pulmonary Fibrosis in Mice. In: *American Journal of Respiratory and Critical Care Medicine* 180 (5), S. 424–436. DOI: 10.1164/rccm.200811-1794OC.

Han, Tao; **Chi**, Ming; Wang, Yan; Mei, Yabo; Li, Qiuping; Yu, Mengnan et al. (2017): Therapeutic effects of fibroblast growth factor-10 on hyperoxia-induced bronchopulmonary dysplasia in neonatal mice. In: *American Journal of Translational Research* 9 (8), S. 3528–3540.

Hines, Elizabeth A.; **Sun**, Xin (2014): Tissue crosstalk in lung development. In: *Journal of cellular biochemistry* 115 (9), S. 1469–1477. DOI: 10.1002/jcb.24811.

Hokuto, Isamu; **Perl**, Anne-Karina T.; Whitsett, Jeffrey A. (2003): Prenatal, but not postnatal, inhibition of fibroblast growth factor receptor signaling causes emphysema. In: *The Journal of biological chemistry* 278 (1), S. 415–421. DOI: 10.1074/jbc.M208328200.

Hou, Ana; **Fu**, Jianhua; Yang, Haiping; Zhu, Yuting; Pan, Yuqing; Xu, Shuyan; Xue, Xindong (2015): Hyperoxia stimulates the transdifferentiation of type II alveolar epithelial cells in newborn rats. In: *American journal of physiology. Lung cellular and molecular physiology* 308 (9), L861-72. DOI: 10.1152/ajplung.00099.2014.

Husain, Aliya N.; **Siddiqui**, Noman H.; Stocker, J.Thomas (1998): Pathology of arrested acinar development in postsurfactant bronchopulmonary dysplasia. In: *Human Pathology* 29 (7), S. 710–717. DOI: 10.1016/S0046-8177(98)90280-5.

Igarashi, M.; **Finch**, P. W.; Aaronson, S. A. (1998): Characterization of recombinant human fibroblast growth factor (FGF)-10 reveals functional similarities with keratinocyte growth factor (FGF-7). In: *The Journal of biological chemistry* 273 (21), S. 13230–13235. DOI: 10.1074/jbc.273.21.13230.

Ikonomou, Laertis; **Herriges**, Michael J.; Lewandowski, Sara L.; Marsland, Robert; Villacorta-Martin, Carlos; Caballero, Ignacio S. et al. (2020): The in vivo genetic

program of murine primordial lung epithelial progenitors. In: *Nature communications* 11 (1), S. 635. DOI: 10.1038/s41467-020-14348-3

Itoh, Nobuyuki; **Ornitz**, David M. (2008): Functional evolutionary history of the mouse Fgf gene family. In: *Developmental dynamics : an official publication of the American Association of Anatomists* 237 (1), S. 18–27. DOI: 10.1002/dvdy.21388.

Itoh, Nobuyuki; **Ornitz**, David M. (2011a): Fibroblast growth factors. From molecular evolution to roles in development, metabolism and disease. In: *Journal of biochemistry* 149 (2), S. 121–130. DOI: 10.1093/jb/mvq121.

Itoh, Nobuyuki; **Ornitz**, David M. (2011b): Fibroblast growth factors: from molecular evolution to roles in development, metabolism and disease. In: *Journal of biochemistry* 149 (2), S. 121–130. DOI: 10.1093/jb/mvq121.

Jacob, Anjali; **Morley**, Michael; Hawkins, Finn; McCauley, Katherine B.; Jean, J. C.; Heins, Hillary et al. (2017): Differentiation of Human Pluripotent Stem Cells into Functional Lung Alveolar Epithelial Cells. In: *Cell stem cell* 21 (4), 472-488.e10. DOI: 10.1016/j.stem.2017.08.014.

Jones, Matthew R.; **Dilai**, Salma; Lingampally, Arun; Chao, Cho-Ming; Danopoulos, Soula; Carraro, Gianni et al. (2018): A Comprehensive Analysis of Fibroblast Growth Factor Receptor 2b Signaling on Epithelial Tip Progenitor Cells During Early Mouse Lung Branching Morphogenesis. In: *Frontiers in Genetics* 9, S. 746. DOI: 10.3389/fgene.2018.00746.

Jones, Matthew R.; **Lingampally**, Arun; Wu, Jin; Sedighi, Jamschid; Ahmadvand, Negah; Wilhelm, Jochen et al. (2020): Evidence for Overlapping and Distinct Biological Activities and Transcriptional Targets Triggered by Fibroblast Growth Factor Receptor 2b Signaling between Mid- and Early Pseudoglandular Stages of Mouse Lung Development. In: *Cells* 9 (5). DOI: 10.3390/cells9051274.

Kalikkot Thekkeveedu, Renjithkumar; **Guaman**, Milenka Cuevas; Shivanna, Binoy (2017): Bronchopulmonary dysplasia: A review of pathogenesis and pathophysiology. In: *Respiratory medicine* 132, S. 170–177. DOI: 10.1016/j.rmed.2017.10.014.

Kalinina, Juliya; **Dutta**, Kaushik; Ilghari, Dariush; Beenken, Andrew; Goetz, Regina; Eliseenkova, Anna V. et al. (2012): The alternatively spliced acid box region plays a key role in FGF receptor autoinhibition. In: *Structure(London, England:1993)* 20 (1), S. 77–88. DOI: 10.1016/j.str.2011.10.022.

Klar, Joakim; **Blomstrand**, Peter; Brunmark, Charlott; Badhai, Jitendra; Håkansson, Hanna Falk; Brange, Charlotte Sollie et al. (2011): Fibroblast growth factor 10 haploinsufficiency causes chronic obstructive pulmonary disease. In: *Journal of medical genetics* 48 (10), S. 705–709. DOI: 10.1136/jmedgenet-2011-100166.

Knust, Juliane; **Ochs**, Matthias; Gundersen, Hans Jørgen G.; Nyengaard, Jens R. (2009): Stereological estimates of alveolar number and size and capillary length and surface area in mice lungs. In: *Anatomical record (Hoboken, N.J. : 2007)* 292 (1), S. 113–122. DOI: 10.1002/ar.20747.

Kresch, M. J.; **Christian**, C.; Wu, F.; Hussain, N. (1998): Ontogeny of apoptosis during lung development. In: *Pediatric research* 43 (3), S. 426–431. DOI: 10.1203/00006450-199803000-00021.

Langhe, Stijn P. de; **Carraro**, Gianni; Warburton, David; Hajihosseini, Mohammad K.; Bellusci, Saverio (2006): Levels of mesenchymal FGFR2 signaling modulate smooth muscle progenitor cell commitment in the lung. In: *Developmental Biology* 299 (1), S. 52–62. DOI: 10.1016/j.ydbio.2006.07.001.

MacArthur, C. A.; **Lawshé**, A.; Xu, J.; Santos-Ocampo, S.; Heikinheimo, M.; Chellaiah, A. T.; Ornitz, D. M. (1995): FGF-8 isoforms activate receptor splice forms that are expressed in mesenchymal regions of mouse development. In: *Development (Cambridge, England)* 121 (11), S. 3603–3613. Online verfügbar unter https://dev.biologists.org/content/121/11/3603.short.

MacKenzie, BreAnne; **Henneke**, Ingrid; Hezel, Stefanie; Al Alam, Denise; El Agha, Elie; Chao, Cho-Ming et al. (2015): Attenuating endogenous Fgfr2b ligands during bleomycin-induced lung fibrosis does not compromise murine lung repair. In: *American journal of physiology. Lung cellular and molecular physiology* 308 (10), L1014-24. DOI: 10.1152/ajplung.00291.2014.

Makanya, Andrew; **Anagnostopoulou**, Aikaterini; Djonov, Valentin (2013): Development and remodeling of the vertebrate blood-gas barrier. In: *BioMed research international* 2013, S. 101597. DOI: 10.1155/2013/101597.

Mansukhani, A.; **Dell'Era**, P.; Moscatelli, D.; Kornbluth, S.; Hanafusa, H.; Basilico, C. (1992): Characterization of the murine BEK fibroblast growth factor (FGF) receptor: activation by three members of the FGF family and requirement for heparin. In: *Proceedings of the National Academy of Sciences of the United States of America* 89 (8), S. 3305–3309. DOI: 10.1073/pnas.89.8.3305.

Mathew, Rajamma (2020): Signaling Pathways Involved in the Development of Bronchopulmonary Dysplasia and Pulmonary Hypertension. In: *Children* 7 (8). DOI: 10.3390/children7080100.

Miki, T.; **Bottaro**, D. P.; Fleming, T. P.; Smith, C. L.; Burgess, W. H.; Chan, A. M.; Aaronson, S. A. (1992): Determination of ligand-binding specificity by alternative splicing: two distinct growth factor receptors encoded by a single gene. In: *Proceedings of the National Academy of Sciences of the United States of America* 89 (1), S. 246–250. DOI: 10.1073/pnas.89.1.246.

Mohammadi, Moosa; **Olsen**, Shaun K.; Ibrahimi, Omar A. (2005): Structural basis for fibroblast growth factor receptor activation. In: *Cytokine & growth factor reviews* 16 (2), S. 107–137. DOI: 10.1016/j.cytogfr.2005.01.008.

Moore, Keith L.; **Persaud**, Trivedi V. N.; Torchia, Mark G. (2016): The developing human. Clinically oriented embryology. 10th edition. Philadelphia, PA: Elsevier.

Nyeng, Pia; **Norgaard**, Gitte A.; Kobberup, Sune; Jensen, Jan (2008): FGF10 maintains distal lung bud epithelium and excessive signaling leads to progenitor state arrest, distalization, and goblet cell metaplasia. In: *BMC developmental biology* 8, S. 2. DOI: 10.1186/1471-213X-8-2.

Ornitz, D. M.; **Leder**, P. (1992): Ligand specificity and heparin dependence of fibroblast growth factor receptors 1 and 3. In: *The Journal of biological chemistry* 267 (23), S. 16305–16311.

Ornitz, David M.; **Itoh**, Nobuyuki (2015a): The Fibroblast Growth Factor signaling pathway. In: *Wiley interdisciplinary reviews. Developmental biology* 4 (3), S. 215–266. DOI: 10.1002/wdev.176.

Ornitz, David M.; **Itoh**, Nobuyuki (2015b): The Fibroblast Growth Factor signaling pathway. In: *Wiley interdisciplinary reviews. Developmental biology* 4 (3), S. 215–266. DOI: 10.1002/wdev.176.

Owen, Louise S.; **Manley**, Brett J.; Davis, Peter G.; Doyle, Lex W. (2017): The evolution of modern respiratory care for preterm infants. In: *The Lancet* 389 (10079), S. 1649–1659. DOI: 10.1016/S0140-6736(17)30312-4.

Parsa, Sara; **Kuremoto**, Koh-ichi; Seidel, Kerstin; Tabatabai, Reza; MacKenzie, BreAnne; Yamaza, Takayoshi et al. (2010): Signaling by FGFR2b controls the regenerative capacity of adult mouse incisors. In: *Development* 137 (22), S. 3743–3752. DOI: 10.1242/dev.051672.

Parsa, Sara; **Ramasamy**, Suresh K.; Langhe, Stijn De; Gupte, Varsha V.; Haigh, Jody J.; Medina, Daniel; Bellusci, Savério (2008): Terminal end bud maintenance in mammary gland is dependent upon FGFR2b signaling. In: *Developmental Biology* 317 (1), S. 121–131. DOI: 10.1016/j.ydbio.2008.02.014.

Perl, Anne-Karina T.; **Gale**, Emily (2009): FGF signaling is required for myofibroblast differentiation during alveolar regeneration. In: *American journal of physiology. Lung cellular and molecular physiology* 297 (2), L299-308. DOI: 10.1152/ajplung.00008.2009.

Ramasamy, Suresh K.; **Mailleux**, Arnaud A.; Gupte, Varsha V.; Mata, Francisca; Sala, Frédéric G.; Veltmaat, Jacqueline M. et al. (2007): Fgf10 dosage is critical for the amplification of epithelial cell progenitors and for the formation of multiple mesenchymal lineages during lung development. In: *Developmental Biology* 307 (2), S. 237–247. DOI: 10.1016/j.ydbio.2007.04.033.

Rawlins, Emma L. (2008): Lung epithelial progenitor cells: lessons from development. In: *Proceedings of the American Thoracic Society* 5 (6), S. 675–681. DOI: 10.1513/pats.200801-006AW.

Rawlins, Emma L.; **Clark**, Cheryl P.; Xue, Yan; Hogan, Brigid L. M. (2009): The Id2+ distal tip lung epithelium contains individual multipotent embryonic progenitor cells. In: *Development (Cambridge, England)* 136 (22), S. 3741–3745. DOI: 10.1242/dev.037317.

Scheckenbach, Kathrin; **Balz**, Vera; Wagenmann, Martin; Hoffmann, Thomas K. (2008): An intronic alteration of the fibroblast growth factor 10 gene causing ALSG-(aplasia of lacrimal and salivary glands) syndrome. In: *BMC Medical Genetics* 9, S. 114. DOI: 10.1186/1471-2350-9-114.

Schittny, Johannes C. (2017): Development of the lung. In: *Cell and Tissue Research* 367 (3), S. 427–444. DOI: 10.1007/s00441-016-2545-0.

Schittny, Johannes C.; **Mund**, Sonja I.; Stampanoni, Marco (2008): Evidence and structural mechanism for late lung alveolarization. In: *American journal of physiology. Lung cellular and molecular physiology* 294 (2), L246-54. DOI: 10.1152/ajplung.00296.2007.

Sekine, K.; **Ohuchi**, H.; Fujiwara, M.; Yamasaki, M.; Yoshizawa, T.; Sato, T. et al. (1999): Fgf10 is essential for limb and lung formation. In: *Nature genetics* 21 (1), S. 138–141. DOI: 10.1038/5096.

Shams, Imad; **Rohmann**, Edyta; Eswarakumar, Veraragavan P.; Lew, Erin D.; Yuzawa, Satoru; Wollnik, Bernd et al. (2007): Lacrimo-auriculo-dento-digital syndrome is caused by reduced activity of the fibroblast growth factor 10 (FGF10)-FGF receptor 2 signaling pathway. In: *Molecular and Cellular Biology* 27 (19), S. 6903–6912. DOI: 10.1128/MCB.00544-07.

Szebenyi, G.; **Fallon**, J. F. (1999): Fibroblast growth factors as multifunctional signaling factors. In: *International review of cytology* 185, S. 45–106. DOI: 10.1016/s0074-7696(08)60149-7.

Taylor, Kristen R.; **Rudisill**, Jennifer A.; Gallo, Richard L. (2005): Structural and sequence motifs in dermatan sulfate for promoting fibroblast growth factor-2 (FGF-2) and FGF-7 activity. In: *The Journal of biological chemistry* 280 (7), S. 5300–5306. DOI: 10.1074/jbc.M410412200.

Treutlein, Barbara; **Brownfield**, Doug G.; Wu, Angela R.; Neff, Norma F.; Mantalas, Gary L.; Espinoza, F. Hernan et al. (2014): Reconstructing lineage hierarchies of the distal lung epithelium using single-cell RNA-seq. In: *Nature* 509 (7500), S. 371–375. DOI: 10.1038/nature13173.

Volckaert, Thomas; **Campbell**, Alice; Dill, Erik; Li, Changgong; Minoo, Parviz; Langhe, Stijn De (2013): Localized Fgf10 expression is not required for lung branching morphogenesis but prevents differentiation of epithelial progenitors. In: *Development* 140 (18), S. 3731–3742. DOI: 10.1242/dev.096560.

Volckaert, Thomas; **Dill**, Erik; Campbell, Alice; Tiozzo, Caterina; Majka, Susan; Bellusci, Saverio; Langhe, Stijn P. de (2011): Parabronchial smooth muscle

constitutes an airway epithelial stem cell niche in the mouse lung after injury. In: *The Journal of Clinical Investigation* 121 (11), S. 4409–4419. DOI: 10.1172/JCI58097.

Voynow, Judith A. (2017): "New" bronchopulmonary dysplasia and chronic lung disease. In: *Paediatric respiratory reviews* 24, S. 17–18. DOI: 10.1016/j.prrv.2017.06.006.

Wang, Yi; **Frank**, David B.; Morley, Michael P.; Zhou, Su; Wang, Xiaoru; Lu, Min Min et al. (2016): HDAC3-Dependent Epigenetic Pathway Controls Lung Alveolar Epithelial Cell Remodeling and Spreading via miR-17-92 and TGF-β Signaling Regulation. In: *Developmental Cell* 36 (3), S. 303–315. DOI: 10.1016/j.devcel.2015.12.031.

Weinstein, M.; **Xu**, X.; Ohyama, K.; Deng, C. X. (1998): FGFR-3 and FGFR-4 function cooperatively to direct alveogenesis in the murine lung. In: *Development (Cambridge, England)* 125 (18), S. 3615–3623.

Wendel, D. P.; **Taylor**, D. G.; Albertine, K. H.; Keating, M. T.; Li, D. Y. (2000): Impaired distal airway development in mice lacking elastin. In: *American journal of respiratory cell and molecular biology* 23 (3), S. 320–326. DOI: 10.1165/ajrcmb.23.3.3906.

Wong, Chi Heem; **Siah**, Kien Wei; Lo, Andrew W. (2019): Estimation of clinical trial success rates and related parameters. In: *Biostatistics (Oxford, England)* 20 (2), S. 273–286. DOI: 10.1093/biostatistics/kxx069.

Wu, Xinle; **Ge**, Hongfei; Lemon, Bryan; Vonderfecht, Steven; Weiszmann, Jennifer; Hecht, Randy et al. (2010): FGF19-induced hepatocyte proliferation is mediated through FGFR4 activation. In: *The Journal of biological chemistry* 285 (8), S. 5165–5170. DOI: 10.1074/jbc.M109.068783.

XING, YUJIAO; **Fu**, Jianhua; Yang, Haiping; Yao, Li; Qiao, Lin; DU, YANNA; Xue, Xindong (2015): MicroRNA expression profiles and target prediction in neonatal Wistar rat lungs during the development of bronchopulmonary dysplasia. In: *Int J Mol Med* 36 (5), S. 1253–1263. DOI: 10.3892/ijmm.2015.2347.

Yoshida, Masao; **Meguro**, Akira; Okada, Eiichi; Nomura, Naoko; Mizuki, Nobuhisa (2013): Association study of fibroblast growth factor 10 (FGF10) polymorphisms

with susceptibility to extreme myopia in a Japanese population. In: *Molecular Vision* 19, S. 2321–2329.

Yuan, Tingting; **Volckaert**, Thomas; Redente, Elizabeth F.; Hopkins, Seantel; Klinkhammer, Kylie; Wasnick, Roxana et al. (2019): FGF10-FGFR2B Signaling Generates Basal Cells and Drives Alveolar Epithelial Regeneration by Bronchial Epithelial Stem Cells after Lung Injury. In: *Stem Cell Reports* 12 (5), S. 1041–1055. DOI: 10.1016/j.stemcr.2019.04.003.

9. SUPPLEMENTARY DATA

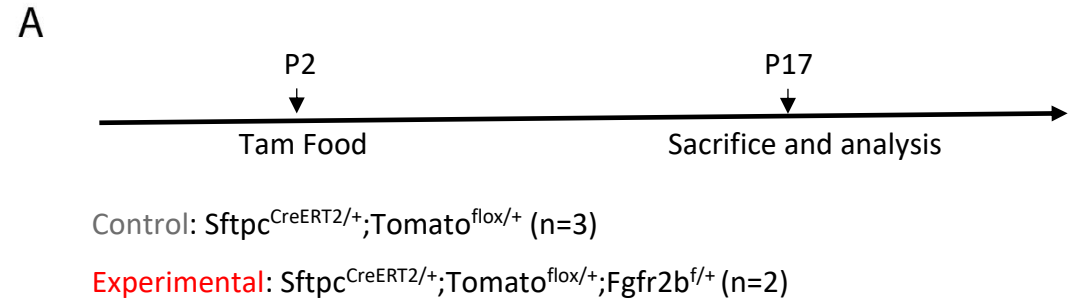

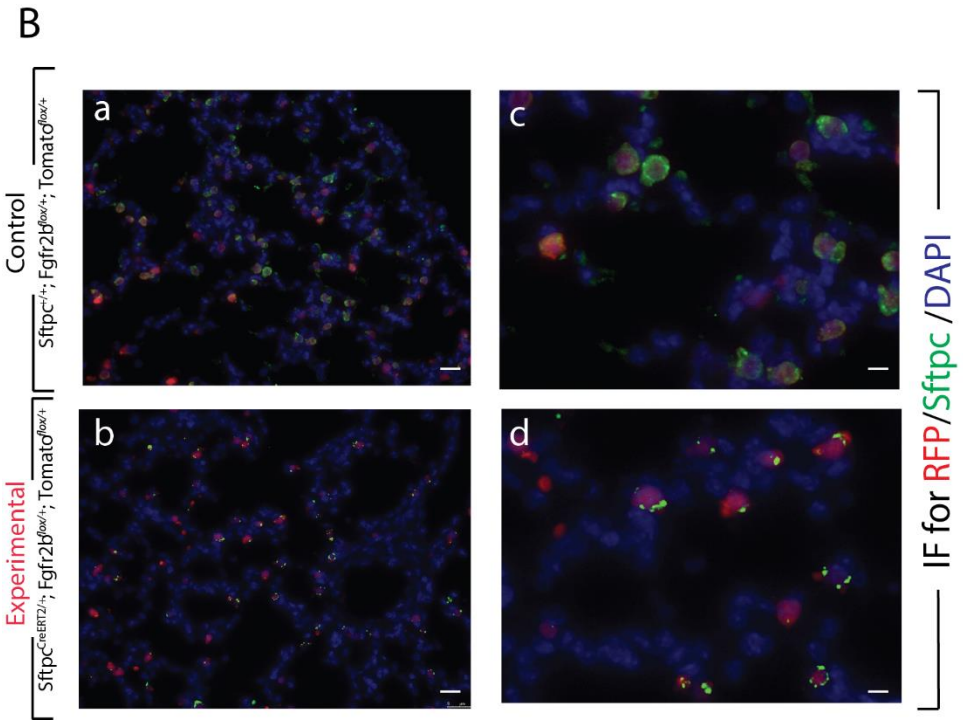

Figure S1: Sftpc-staining in triple transgenic mouse model (*Sftpc$^{CreERT2/+}$;Tomato$^{flox/+}$;Fgfr2b$^{flox/+}$*) at P17.

(**A**) Experimental approach. Only one of the 3 control lungs is RFP+. (**B**) Immunofluorescence staining for Sftpc at P17. The red cells are Tomato+ cells. Note the decrease of Sftpc in the Tomato+ cells in the experimental (n=2) (**b,d**) versus control (n=1) (**a,c**) lungs. Here we want to show our Sftpc-staining at P17 with only one RFP+ control mouse. We had only 1 lung in our control group, which was RFP+. Nevertheless,

we did a double staining with RFP and Sftpc to detect the effect of Sftpc in the AEC II cells. Although the number of the control group was just one individuum, we could still see a decrease of Sftpc in the experimental lungs (n=2) versus our control lung (n=1). A quantification was unfortunately not useful by just one control mouse. But here we can see a trend. Further experiments at this stage will be necessary to investigate the complex Fgf10/Fgfr2b mechanism in *Sftpc*-positive cells.

Scale bar for Ba,b, 75 µm, Bc,d 30 µm.

10. PUBLICATIONS

Jones, Matthew R.; Lingampally, Arun; Wu, Jin; **Sedighi, Jamschid**; Ahmadvand, Negah; Wilhelm, Jochen et al. (**2020**): Evidence for Overlapping and Distinct Biological Activities and Transcriptional Targets Triggered by Fibroblast Growth Factor Receptor 2b Signaling between Mid- and Early Pseudoglandular Stages of Mouse Lung Development. In: *Cells* 9 (5). DOI: 10.3390/cells9051274.

Chao, Cho-Ming; Carraro, Gianni; Rako, Zvonimir A.; Kolck, Johannes; **Sedighi, Jamschid**; Zimmermann, Volker et al. (**2020**): Failure to Down-Regulate miR-154 Expression in Early Postnatal Mouse Lung Epithelium Suppresses Alveologenesis, with Changes in Tgf-β Signaling Similar to those Induced by Exposure to Hyperoxia. In: *Cells* 9 (4), S. 859. DOI: 10.3390/cells9040859. (Chao et al. 2020)

11. ACKNOWLEDGMENTS

I would like to thank everyone who assisted and supported me along the way to completing this doctoral thesis.

First of all, I would like to thank PD Dr. Cho-Ming Chao, PhD for giving me the opportunity to work on my doctoral thesis and the insight that he gave to me into basic research. The completion of this doctoral thesis would not have been possible without his support and motivation throughout the whole thesis process. He has always provided outstanding advice and I am thankful for his constant friendliness and incredible patience.

The same gratitude I would like to express to Prof. Dr. Saverio Bellusci, the head of the Bellusci laboratory. I am deeply grateful for his optimism and his friendliness towards students. His enthusiasm and passion encouraged and inspired me throughout my work.

Secondly, I would like to thank Kerstin Goth and Heike Habermann for their friendly administrative help. As a lab manager, Kerstin has always been there for me and I am very thankful for her expertise. Kerstin and Saverio also gave me the opportunity to work as a student assistant to support myself during my studies.

I would also like to acknowledge the other students and members in the Bellusci lab team, Matt Jones, Alena Moiseenko, Amit Shrestha, Jana Rostkovius, Negah Ahmadvand, Vahid Kheirollahi, Sara Taghizadeh, Zvonimir Rako, Johannes Kolck and Volker Zimmermann. You have all been great colleagues and I am really thankful to get the opportunity to work with you. I would like to express my special thanks to Jana, the person who supported me throughout genotyping many mice. Also special thanks to Zvonimir, who gave me the motivation to finish this doctoral thesis and helped me to correct this work. You all contribute to the great working atmosphere at the Bellusci lab.

Finally, I would like to express my deep thanks and love to my parents who have always supported me unconditionally. You are the reason why I am where I am now. I am dedicating this doctoral thesis to give you a little bit of something back, but it will never be enough compared to what you have given me.

Furthermore, I am very thankful to my brother Zohoor, his wife Fatima, my brother Haron and my sister Serena. I also thank my parents-in-law Davoud and Liza Sahebzada. You gave me the women who supports me endlessly and is always by my side.

Last but not the least, I would like to show my deepest gratitude to all the mice that were sacrificed for the completion of my doctoral thesis.

12. CURRICULUM VITAE